Leveraging Modeling and Sensitivity Studies for Improving Aerodynamic Predictions for Multirotor Aircraft

Dorsa Shirazi
Aerospace Engineer
NASA Ames Research Center
Moffett Field, CA, U.S.

Nicholas Peters
Aerospace Engineer
NASA Ames Research Center
Moffett Field, CA, U.S.

Carl Russell
Chief, Aeromechanics Office
NASA Ames Research Center
Moffett Field, CA, U.S.

Sarah Conley
Mechanical Engineer
NASA Ames Research Center
Moffett Field, CA, U.S.

Kristen Kallstrom
Aerospace Engineer
NASA Ames Research Center
Moffett Field, CA, U.S.

Carlos Pereyra
Aerospace Engineer
NASA Ames Research Center
Moffett Field, CA, U.S.

Stephen Wright
Aerospace Engineer
NASA Ames Research Center
Moffett Field, CA, U.S.

Jordan Mills
Aerospace Student
Embry-Riddle Aeronautical University
Daytona Beach, FL, U.S.

ABSTRACT

The NASA Revolutionary Vertical Lift Technology project aims to support and guide the development of vertical flight vehicles for the benefit of the U.S. rotorcraft community and to increase the quality of life of the public. As part of this effort, the Multirotor Test Bed (MTB) – designed and built by NASA – has been tested twice at the U.S. Army 7- by 10-Foot Wind Tunnel at NASA Ames Research Center in 2019 (MTB1) and 2022 (MTB2). This study utilizes MTB2 experimental data for sensitivity studies on rotor aerodynamic performance of a quadrotor configuration using two mid-fidelity tools, the Comprehensive Hierarchical Aeromechanics Rotorcraft Model (CHARM) as well as Blade Element Theory based disk modeling in the OVERFLOW CFD solver. Additionally, this study leverages analyzing computational rotor performance predictions with experimental data to help identify future test configurations for the upcoming MTB3 test in the National Full-Scale Aerodynamics Complex 40- by 80-Foot Wind Tunnel.

NOTATION

$\hat{C}$	resultant calibration coefficients
C_T	thrust coefficient
C_Q	torque coefficient
$\hat{F}$	mean load prediction via conversion model
F_x	force reading from load cell in x-direction, lb
F_y	force reading from load cell in y direction, lb
F_z	thrust force reading from load cell, lb
M_x	roll moment reading from load cell, in-lb
M_y	pitch moment reading from load cell, in-lb
M_z	torque reading from load cell, in-lb
R	blade radius, ft
$R1$	fore starboard rotor 1
$R2$	fore port rotor 2
$R3$	aft port rotor 3
$R4$	aft starboard rotor 4
Re/M	Reynolds Mach ratio
dz	height difference between the fore and aft rotors
t/c	maximum thickness-to-chord ratio
a_1	diffusion gain constant
r_{c_0}	initial element core size, ft
u_{dyn}	dynamic uncertainty
$u_{pi,95}$	uncertainty, 95% of predictive interval
u_{tot}	total uncertainty
$\hat{V}$	voltage, V
μ	advance ratio
σ	load cell variance
ν	kinematic viscosity, ft^2/s
Γ_v	vortex circulation strength, ft^2/s
BET	blade element theory
BCVE	basic curved vortex elements
CFD	computational fluid dynamics
CVC	constant vorticity contour
HFV	hierarchical fast vortex method
RTDs	resistance temperature detectors
RVLT	Revolutionary Vertical Lift Technology
SDAS	data acquisition system
UAM	Urban Air Mobility
VTOL	Vertical Take-Off and Landing

Presented at the Vertical Flight Society's 81st Annual Forum & Technology Display, Virginia Beach, VA, USA, May 20–22, 2025.

INTRODUCTION

Urban Air Mobility (UAM) has garnered significant interest from private companies and government aviation departments as an efficient transportation solution in the 21st century. Comprehensive analysis tools and computational fluid dynamics (CFD) can be used to assist in early stage UAM vehicle designs to reduce cost and improve time efficiency by providing informed, high fidelity predictions of rotor performance and rotor wake interactions. Several current UAM designs involve multiple rotors, thus increasing the importance of rotor wake (and rotor-rotor) interactions. To validate Vertical Take-Off and Landing (VTOL) aircraft performance prediction codes across a broad range of vehicle configurations, multiple high-quality sets of rotor performance data are required. Many aircraft companies are currently pursuing multirotor vehicle configuration designs, creating a need for validation data for multirotor systems (Ref. 1). The NASA Multirotor Test Bed (MTB) was designed to actively accommodate a broad range of reconfigurable multirotor systems and measure rotor performance and loads in a wind tunnel environment.

This paper compares simulations results with experimental data obtained during the second MTB wind tunnel test entry, MTB2. The MTB2 wind tunnel test was focused on a quadrotor configuration, with variations in rotor placement, blade number, and rotor phasing for a range of test conditions.

Multirotor Test Bed

The MTB project started with the goal of creating an adjustable test bed to study multirotor configurations by measuring rotor performance, acoustics, and aerodynamic interactions. The MTB consists of up to six individual rotor systems, each with longitudinal, lateral, vertical, and rotational adjustment systems. Each rotor/motor system is mounted on a six-axis load cell to measure both steady and vibratory rotor forces and moments. The MTB assembly can pitch 30° forward and 10° aft. Each rotor can tilt 90° forward and 10° aft. The longitudinal rotor spacing is between 25.5 and 72.0 inches, with adjustment increments of 1.5 inches. The lateral spacing between rotors varies between 24.7 inches and 38.7 inches in 1.0-inch increments. Additionally, the vertical position of the rotors can be raised up to 9.0 inches in 1.0 inch increments

Multirotor Test Bed Entry 1

The first wind tunnel test entry of the MTB system occurred in October 2019 in the U.S. Army 7- by 10-Foot Wind Tunnel at NASA Ames Research Center (Ref. 2). The rotor used for the MTB1 test was an off-the-shelf KDE-CF245-DP with a 24.5-inch diameter. The MTB1 test was primarily a shakedown of the new test hardware to evaluate its ability to operate at different test conditions that included variations in RPM, MTB assembly pitch, wind tunnel air speed, and number of rotors.

Multirotor Test Bed Entry 2

The second wind tunnel entry, MTB2, was completed in August 2022 in the U.S. Army 7- by 10-Foot Wind Tunnel, Figure 1. The MTB2 test was intended to focus on a scaled-down version of the Revolutionary Vertical Lift Technology (RVLT) quadrotor conceptual vehicle configuration (Ref. 3) with variable height of the aft rotors to investigate the effects on rotor performance due to rotor-rotor interference. The three quadrotor configurations were tested with difference in height between the fore and aft rotors of dz/R = 0.33, 0.00, and 0.57. In addition to the variable rotor heights, the MTB2 test included the ability to control the azimuthal phase angle between rotors. Rotor phase angle control has been proposed by various researchers as a method to improve overall vehicle performance and reduce noise and vibrations (Ref. 4).

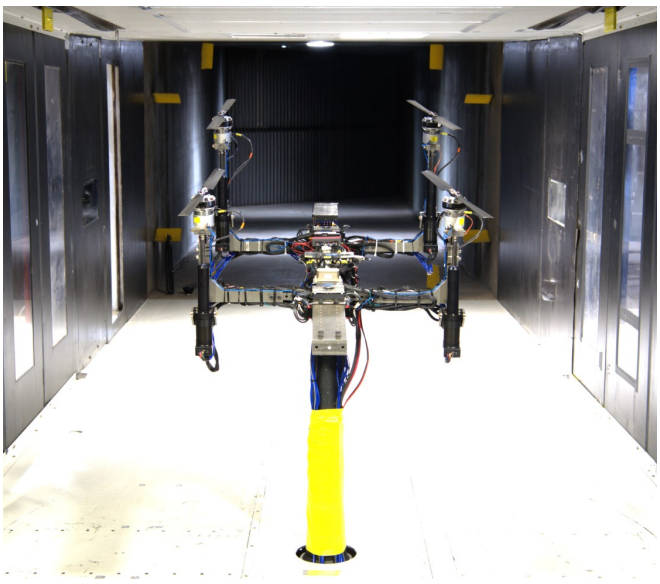

Figure 1. MTB2 in the U.S. Army 7- by 10-Foot Wind Tunnel at NASA Ames Research Center.

Multirotor Test Bed Entry 3

Additional MTB tests are planned in the future, one of will focus on the evaluation of noise produced by multirotor systems at model- and full-scale. The third MTB wind tunnel test entry (MTB3) is planned to take place in the National Full-Scale Aerodynamics Complex (NFAC) in 2026 and will provide the ability to measure noise in an anechoic facility. MTB3 will include previous model capabilities and a new hub with ground adjustable collective. The blades used in MTB2 will be tested along with new blades to provide additional data for comparison between test campaigns. The MTB3 rotor will retain the MTB2 rotor diameter of 24.5-inch for both blade sets. Future testing after MTB3 will focus on a larger multirotor system that will provide research data on the effects of scaling.

TEST DESCRIPTION

U.S Army 7- by 10-Foot Wind Tunnel

The MTB2 test was conducted in the U.S. Army 7- by 10-Foot Wind Tunnel at NASA Ames Research Center. This is a closed-throat, single-return wind tunnel with a 14:1 contraction ratio, with a test section of 7.0 x 10.0 x 15.0 feet. Test stands are generally mounted on struts and secured to the turntable in the center of the test section. The Standard Data Acquisition System (SDAS) is the primary data acquisition software and includes a LabVIEW-based interface. SDAS uses a flexible architecture to acquire a large number of channels – channel count and acquisition speed are based on the data acquisition hardware present at any given time.

Test Matrix of the MTB2 Tunnel Entry

During the MTB2 test campaign, the longitudinal and lateral rotor spacing on the stand was kept constant at 2.750 ft and 2.725 ft, respectively, and only vertical spacing was varied. Table 1 summarizes the test variables for MTB2.

Table 1. MTB2 test variables.

Parameter	Value
Number of rotors	1,2[a],4[b]
Number of blades	2, 3, 6
Rotor speeds	2000, 2500, 3000 RPM
Tunnel speeds	0, 20, 40 ft/s
Model pitch (+ aft)	0, -1, -3, -5, -10 deg
Rotor tilt (+ forward)	0, -3 deg
Phase	0, -30, -45, -60, -90 deg
Vertical rotor spacing (dz/R)	0.00, 0.33, 0.57

[a]Tandem and side-by-side configuration
[b]Quadrotor at dz/R= 0.00, 0.33, and 0.57

Note that the 3-bladed and 6-bladed runs for the conceptual quadrotor configuration (dz/R = 0.33) were not performed for all possible testing conditions. While Table 1 provides a general outline of the majority of testing conditions, a more detailed list of test runs can be found in (Ref. 5).

Experimental Data Collection and Correction

The source MTB2 data acquired in the U.S. Army 7- by 10-Foot Wind Tunnel is organized into two types: 1) quasi-static and 2) dynamic. Quasi-static data represent aggregate or mean values derived from the unfiltered dynamic channel measurements. Source dynamic data, of a selected run-point combination, represent a 5 second time-history of hub-load measurements sampled at 4 kHz. As a clarifying point, each selected point index (within a particular run), corresponds to a variation of one of these parameters: 1) tunnel speed, 2) model pitch, 3) rotor tilt, and 4) rotor speed. A selected run index may correspond to a unique rotor configuration. See Data Report (Ref. 5) for the manifest of run conditions and associated parameters. Unaltered quasi-static voltage signals were converted into engineering units based on a custom linear calibration that accounts for Gaussian uncertainties in linear model terms. Adding error bounds on mean (predicted) loads, shown in Equation 1, gives a sense of the possible loading solutions.

$$\hat{F} = V\hat{C} \pm u_{tot}(V) \tag{1}$$

The total uncertainty u_{tot} here represents a combination of random fluctuation (in the calibration set) and mean dynamic uncertainty in each wind-tunnel run-point. A predictive interval derived from deviations in ground truth measurements gives a sense of the upper and lower bounds of potential load values. Generally, $u_{tot} = \sqrt{u_{pi,95\%}^2 + u_{dyn}^2}$ is a magnitude value that may be added symmetrically about the mean load predictions $V\hat{C}$. The first term, $u_{pi,95\%}$, represents the 95% percent predictive interval of a normal linear distribution, for addition detail refer to the AIAA handbook (Ref. 6, section 3.6). Note, the uncertainty depends on the load value (or voltage) which is why u_{tot} is expressed as a function of V. It is known that the conversions yield significant residuals in side force predictions attributed to the sensor's observed channel coupling. Vertical loading however, consistently exhibited the least residuals, which are critical for accurate thrust predictions, as shown in the Table 2. Table 2 illustrates the MTB2 load cell variances and indicates that for load cells 1 and 2, the variance in the thrust direction is nominally higher than in load cells 3 and 4, and thus, may yield higher regions of predictive intervals (larger error bars). Note that all experimental loading values were corrected for time drift, inertial contributions, as well as weight contributions.

Table 2. MTB2 load cell variances.

Load Cell	σ_{F_x} (lb)	σ_{F_y} (lb)	σ_{F_z} (lb)	σ_{M_x} (in-lb)	σ_{M_y} (in-lb)	σ_{M_z} (in-lb)
LC1	0.93	0.19	0.32	0.65	0.82	0.64
LC2	0.08	0.04	0.29	0.14	0.31	0.56
LC3	0.37	0.21	0.08	0.16	0.13	0.08
LC4	0.09	0.08	0.07	0.29	0.22	0.11

Larger variances σ_{F_z} corresponding to Rotor#1 and Rotor#2 may yield larger error bars, particularly when comparing fore and aft rotor aerodynamic performance.

MTB2 REFERENCE BLADE

The rotor blades for MTB1 were procured as Commercial-Off-The-Shelf (COTS) items. For this reason, the rotor blade geometry is not available for public distribution. In alignment with the RVLT goal of supplying data to the aviation community (industry, academia, and Government) to validate its software and use in conceptual design, the rotor blade geometry and airfoil tables for MTB2 were selected and developed at NASA Ames Research Center and will be openly published.

A rectangular rotor blade planform with a constant chord of 1.54 inches, a diameter of 24.48 inches, and a 2.448-inch root

cutout was selected for the MTB2 rotor. The Eppler 387 (E387) airfoil was selected for the entire blade span due to the low Reynolds numbers expected. The airfoil tables were generated first, and a rotor performance study was then completed to analyze different rotor geometries and their effect on rotor performance characteristics (Ref. 5).

MTB2 Airfoil Tables

The Reynolds number for each radial station, from root to tip, was calculated based on expected wind tunnel test conditions, including standard atmospheric conditions and wind tunnel speeds of 20 and 40 ft/s. The nominal hover tip Mach number is 0.2394 with a nominal hover tip Reynolds number of 218,147. The advance ratio, μ, for the 20 ft/s and 40 ft/s tunnel conditions at 2500 RPM is 0.07 and 0.15, respectively. At these low advance ratios, rotor-wake (and rotor-rotor) interactions become important, compared to higher advance ratio conditions where there is less likely for wakes from the fore rotors hitting and rolling up with the wakes of the aft rotors. A Reynolds-Mach ratio (Re/M) was used to scale the Reynolds number with Mach number.

Airfoil tables containing the section lift, drag, and moment coefficients as a function of angle of attack and Mach number were generated using AFTGen with OVERFLOW. AFTGen is a program that provides a Graphical User Interface (GUI) for various flow solvers to calculate the aerodynamic coefficients for user-specified airfoil geometry and flow conditions (Ref. 7). OVERFLOW 2.3d is a high-fidelity Computational Fluid Dynamics (CFD) solver that was used to calculate the 2D section aerodynamic coefficients (Ref. 8). The airfoil tables were generated for Mach 0.0 to 0.5 with an angle of attack ranging from -20 to 20 degrees; however, beyond this range, NACA 0012 airfoil tables were used to extend the angle of attack range to $\pm$180 degrees. The output from AFTGen is an airfoil table in both c81 and .csv formats.

MTB2 Blade Geometry

The E387 airfoil tables generated in AFTGen were used as an input file in a CAMRAD II (Ref. 9) rotor performance analysis aimed at determining acceptable settings of linear twist and built-in collective pitch. The performance analysis yielded a linear twist of -16 degrees with a built-in collective of 6.7 degrees at 0.75R. Table 3 provides details on the MTB2 blade geometry.

SIMULATION TOOLS

This study focuses on the importance of aerodynamic interactions between the MTB2 rotors for different configurations. The analysis tools used to perform the study were: Comprehensive Hierarchical Aeromechanics Rotorcraft Model (CHARM) and OVERFLOW. The comprehensive analysis software CHARM uses a lifting-surface representation for the rotor aerodynamics and uses surface panels to model the wind tunnel walls. For this study, the rotor disk option – instead of fully resolved blades – was used in OVERFLOW. For consistency, both the CHARM and OVERFLOW analyses used the same airfoil performance tables for their respective rotor models.

Table 3. MTB2 rotor blade geometry.

Parameter	Value
Airfoil	Eppler 387
Rotor radius	1.02 ft
Root cutout	0.204 ft
Chord	0.128 ft
Trailing edge thickness	0.0017 ft
Linear twist rate	-16 deg/span
Rotor disk area	3.25 ft^2
Geometric solidity ratio	0.08
Blade pitch at 75% radius	6.7 degrees

CHARM – Panel and Blade Element Method

CHARM (Refs. 10, 11) was developed by Continuum Dynamics, Inc (CDI). CHARM models the aerodynamic and dynamic interactions of the aircraft using a computationally efficient Constant Vorticity Contour (CVC) (Refs. 12, 13) free-vortex wake model within a Hierarchical Fast Vortex/Fast Panel (HFV/HFP) Method (Refs. 14, 15) coupled with a lifting surface, vortex lattice of the rotor blades. The CVC model uses multiple equal-strength vortex filaments comprised of Basic Curved Vortex Elements (BCVE's) (Ref. 16) that lie along contours of constant vorticity to model the trailing vortex sheets along the span of each rotor. The blade loads in CHARM are calculated using a vortex lattice method. The HFV/HFP method utilizes a grouping scheme and multipole approximation to significantly reduce computational time. In the grouping technique, vortices and panels are organized into nested cells, with grids being more refined in high-density areas. The calculation employs multipole expansion and Taylor series extrapolations. Compared to high-fidelity CFD solvers, CHARM requires less CPU usage and memory, enabling simulations to be completed in a shorter amount of time and with reduced computational resources being used. In the CHARM analysis for this study, the MTB2 rotor was characterized as a two-bladed rigid rotor with RPMs of 2000 and 3000. The blade planform had a 1.02 ft radius, 20% cutout, 0.128 ft chord, and -16 degrees of linear washout from the hub to tip with a built-in collective of 6.7 degrees at 0.75R. The rotor blades were modeled with a single row of 80 equal-spaced vortex lattice quadrilaterals with 24 azimuth locations. The CHARM panel method can be used to model the wind tunnel wall effects. The wind tunnel was represented using inviscid incompressible flow. When conducting MTB2 simulations in CHARM, the U.S. Army 7- by 10-Foot Wind Tunnel test section was defined as a traditional closed tunnel with walls, floor, and ceiling. Although the actual test section length of the wind tunnel is 15 ft, the length was set to 50 ft in CHARM

(constant cross-section, without contraction or diffuser), Figure 2.

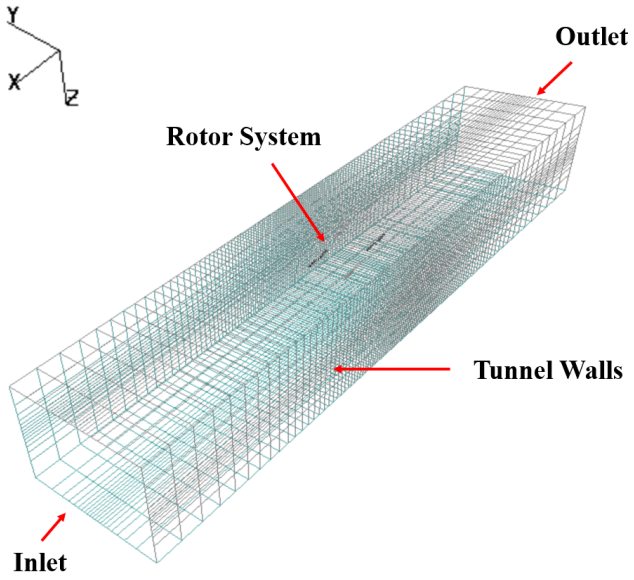

Figure 2. Visualization of the panels used in CHARM for simulating the wind tunnel walls.

OVERFLOW – Rotor Disk Modeling

All CFD simulations conducted in this work utilized the NASA OVERFLOW flow solver (Ref. 8). The OVERFLOW code is an overset, structured grid-based compressible CFD solver frequently employed in the rotorcraft community to achieve high-fidelity predictions for rotorcraft applications (Ref. 17). This study employed the recently implemented Blade Element Theory (BET) source term-based rotor disk model. Each rotor disk was modeled using 50 spanwise nodes and 72 azimuthal nodes for the rotor's CFD mesh. Consistent rotor geometry and airfoil look-up table information was used between the OVERFLOW BET and CHARM models. The solution procedure for the OVERFLOW BET disk model used in this study starts by first extracting CFD computed in-plane and normal velocities at each spanwise and azimuthal node on the rotor disk. The CFD computed in-plane and normal velocities are then used to compute local relative velocities and angles of attack. These values are then used to reference an airfoil performance look-up table such that local lift, drag, and moment coefficients can be computed at each node on the rotor disk. Load coefficients are then converted into source terms and added into the Navier-Stokes energy and momentum equations. For a more comprehensive review, readers are encouraged to review citations (Refs. 18, 19).

All rotor grids were overset with a single-block background mesh. This background mesh initially consisted of a uniform grid refinement region that bounded 0.3 rotor diameters upstream of the fore rotors, 0.3 rotor diameters to the port and starboard of the rotors, 3 rotor diameters downstream the aft rotors, and 0.7 diameters beneath and above the rotors. This uniform refinement region was stretched to match the cross-sectional dimension of the U.S. Army 7- by 10-Foot Wind Tunnel and was extended 20 rotor diameters upstream and downstream of the rotor system. A visual of the grid system for the wind tunnel is shown in Figure 3. All solutions were run with a constant Courant–Friedrichs–Lewy condition prescribed for each grid, run as steady-state simulations, central differencing for the Euler terms, and Beam-Warning scheme for the viscous terms.

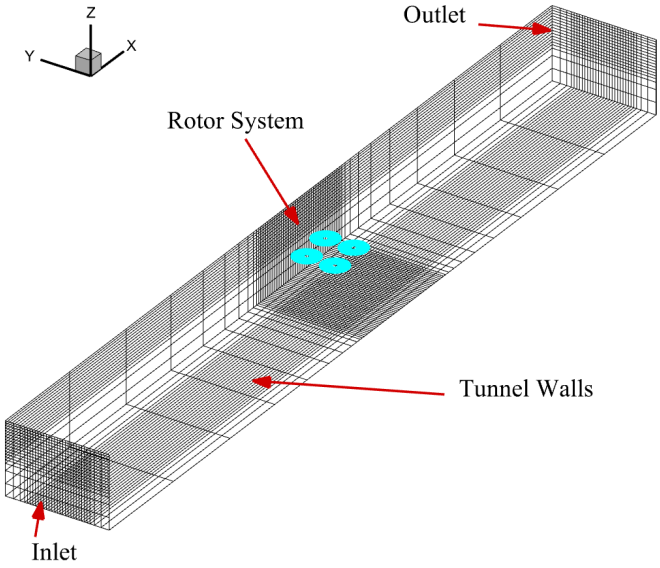

Figure 3. Visualization of the grid system used in OVERFLOW for simulating the quadrotor configuration in this study. For clarity, every fourth node in the grid is shown.

Upstream boundary condition used a velocity inlet, downstream used characteristic outflow condition based on Riemann invariants, and wind tunnel walls were modeled with a pressure extrapolated inviscid adiabatic wall. As will be discussed in the next section, central differencing order accuracy, turbulence model, and background grid refinement were varied to identified solution sensitivity to each said parameters. All CFD simulations were run for 7,000 iterations, which ensured that converged steady-state thrust and power coefficients for all simulations were obtained.

NUMERICAL APPROACH

The conceptual quadrotor (dz/R= 0.33) computational results were utilized for sensitivity studies to capturing rotor-to-rotor and rotor-wake interactions in CHARM and OVERFLOW. Both CHARM and OVERFLOW simulations incorporated the test section walls and utilized the AFTGen-OVERFLOW generated Eppler 387 airfoil tables under the assumption of a rigid blade for multiple revolutions. The simulation predictions shown represent an average over the final 30 revolutions for CHARM and the final 500 iterations for OVERFLOW.

CHARM Sensitivity Study for the Quadrotor

This section outlines the sensitivity study for utilizing CHARM as a mid-fidelity tool to predict the aerodynamic performance for various quadrotor configuration conditions. In this study, four key variables have been identified for a sensitivity analysis of rotor performance using CHARM version 7.3. Table 4 shows the parameters selected, which include the number of surface panels, revolutions, total wake span for the sensitivity analysis, and diffusion gain (a_1). The sensitivity studies were conducted using the conceptual quadrotor experimental data at 2000 and 3000 RPM, with tunnel speeds of 20 and 40 ft/s, rotor tilt angle of 0 deg, and model pitch angles of 0, -5, and -10 degrees.

Table 4. Simulation variables for sensitivity analysis in predicting rotor C_T of quadrotor systems using CHARM.

Parameter	Values
Surface panel resolution	1,700, 6,800, 27,200
# of revolutions	50, 70, 100, 200
Diffusion gain	0.001, 0.005, 0.01, 0.05
# of full-span wake turns	8, 20, 50

CHARM utilizes a surface panel method to model the wind tunnel and allows users to identify the panel numbers in the X, Y, and Z directions. To identify the effect of panel number on capturing the rotor's aerodynamic performance, quadrotor cases were used where the rotor blade was modeled using the vortex lattice method and characterized as a two-bladed rigid rotor. Each sensitivity study case ran for 100 revolutions, and each data point presented in this subsection was an average of the last 30 revolutions.

For the first case study, the U.S. Army 7- by 10-Foot Wind Tunnel test section was modeled with 50, 10, and 7 panels in X, Y, and Z directions with a total of 1,700 panels. In the second case study, the domain dimensions of the tunnel were kept constant while the number of the panels in the X, Y, and Z directions were doubled (100, 20, 14), resulting in a total of 6,800 panels. Finally, for the third-panel sensitivity study, the tunnel was modeled using 200, 40, and 28 panels in X, Y, and Z directions, with 27,200 panels. Table 5 features the mean absolute percentage discrepancy between the CHARM prediction and experimental C_T values for the fore and aft rotors for three cases of a number of panel sensitivity studies. Table 5 shows that the third case study with 27,200 panels was completed in 3 hours, with 0.05% change from the second case study with the 6,800 total panels. The findings from the second case study indicate an improved rotor performance prediction for the fore rotors when compared to the first study case, with a total of 1,700 panels, which requires 1.5 hours to complete. Note that all CHARM cases for the panel study were run using 1 CPU. To further increase the efficiency of the panel method, the U.S. Army 7- by 10-Foot test section was modeled with a concentration of panels near the middle of the tunnel, which decreased the discrepancy between the CHARM prediction and the experimental data by 0.07% for the fore rotors and 0.18% for the aft rotors. Note that the discrepancy percentages presented are the average overall quadrotor configuration at RPMs 2000 and 3000, with tunnel speeds of 20 and 40 ft/s, rotor tilt of 0 deg, and model pitch angles of 0, -5, and -10 degrees. Figure 4 shows the top view of the wake visualization of the conceptual quadrotor (dz/R= 0.33) configuration in the test section, which was modeled using 6,800 panels and with a concentration of panels at the middle of the test section.

Table 5. Rotors 1 and 3 sensitivity to the total panels number selected, shown by mean absolute discrepancy percentage in C_T between experimental measurement and CHARM simulation.

# of Panels	1,700	6,800	27,200
Rotor 1	7.57	7.51	7.47
Rotor 3	6.00	6.06	6.05

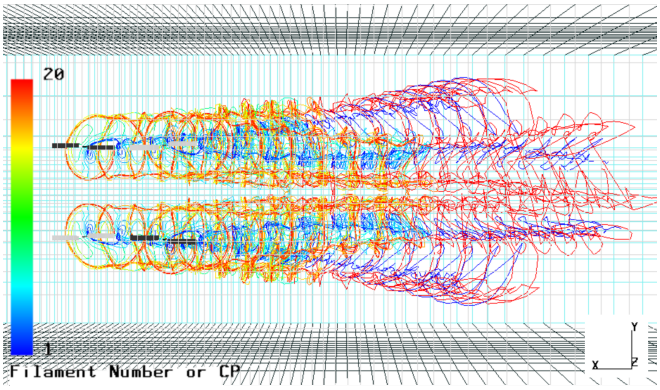

Figure 4. CHARM wake visualization of the conceptual quadrotor configuration in the test section.

The second parameter analyzed in the CHARM sensitivity study for the quadrotor cases was the number of revolutions. A convergence study was initially conducted to examine the variations in the thrust coefficient as a function of the number of revolutions. Figures 5 and 6 illustrate two examples of these convergence studies for the quadrotor cases operating at 3000 RPM and a forward velocity of 40 ft/s, with model pitch angles of -10 and 0 degrees, respectively. Figure 6 shows evidence of unsteady wake during the first ten revolutions, which is particularly pronounced for the aft rotors (R3, R4) due to wake-on-wake interactions occurring between the fore and aft rotors. The findings suggest that after 10 revolutions, the C_T predictions in CHARM stabilize, indicating that utilizing 50 or 70 revolutions may suffice to accurately capture the thrust coefficient by averaging the values over the final 30 revolutions.

Note that the convergence study has been done for all quadrotor cases at RPMs of 2000 and 3000, tunnel speeds of 20 and 40 ft/s, and pitch angles of -10, -5, and 0 degrees. The results

suggest that at 2000 RPM and a tunnel speed of 20 ft/s, the thrust coefficient stabilizes more quickly than at higher RPM and tunnel velocity conditions. However, for consistency across simulation variables, the findings from 3000 RPM, 40 ft/s tunnel speed, and 0 degree pitch angle cases were utilized to establish the adequate number of revolutions for the quadrotor case in CHARM. To examine these findings, each quadrotor case was run with 50, 70, 100, and 200 revolutions, and the induced velocities were calculated and stored at 24 azimuth locations, while the tunnel was modeled using 6,800 panels with higher panel saturation at the middle of the test section. Each data point presented is the average over the last 30 revolutions.

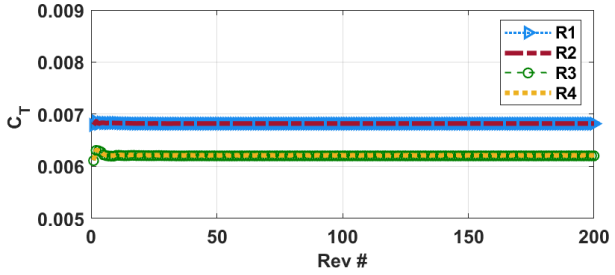

Figure 5. CHARM C_T variation over 200 revolutions for each rotor: Quadrotor at tilt angle of 0 degree and pitch angle of -10 deg, 3000 RPM, 40 ft/s.

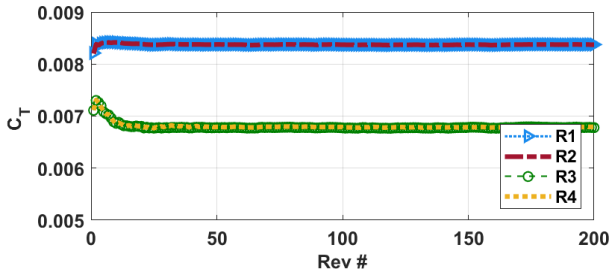

Figure 6. CHARM C_T variation over 200 revolutions for each rotor: Quadrotor at tilt angle of 0 degree and pitch angle of -0 deg, 3000 RPM, 40 ft/s.

Table 6 shows the average discrepancy percentage between the CHARM prediction and the experimental results for the C_T values for the fore and aft rotors. The study cases demonstrate that utilizing 200 revolutions didn't significantly enhances C_T prediction for the fore rotors.

Table 6. Rotor 1 and 3 thrust sensitivity to the number of revolutions selected, shown by mean absolute discrepancy percentage in C_T between experimental measurement and CHARM simulation.

# of Rev	50	70	100	200
Rotor 1	7.49	7.66	7.50	7.50
Rotor 3	6.07	6.08	6.07	6.07

These results may be influenced by the default wake diffusion gain employed by CHARM. CHARM is an inviscid solver, and to account for the diffusion and dissipation of vorticity CHARM used specialized models (Ref. 20), using Eqn 2 to model vortex diffusion, where r_{c_0} is the initial core size of the element, ν is the kinematic viscosity, a_1 is the diffusion gain constant, and Γ_v is the vortex circulation strength.

$$r_c = \sqrt{{r_{c_0}}^2 + 5.0(\nu + a_1\Gamma_v)t} \tag{2}$$

To examine the effect of diffusion gain sensitivity, the thrust sensitivity study was conducted across all quadrotor cases over 100 revolutions. This analysis involved varying the diffusion gain at values of 0.001, 0.005, 0.01, and 0.05. Figure 7 shows the effect of diffusion gain for the quadrotor case at 3000 RPM, 40 ft/s tunnel speed, and 0 degree pitch for the first 50 revolutions. These results show that at lower diffusion gain of 0.001 and 0.005, approximately 20 revolution are required to stabilize C_T. Due to the slower wake dissipation, the fore rotor wake extends and interacts with the wake of the aft rotors. This interactions causes the wakes to roll up, resulting in increased wake instability.

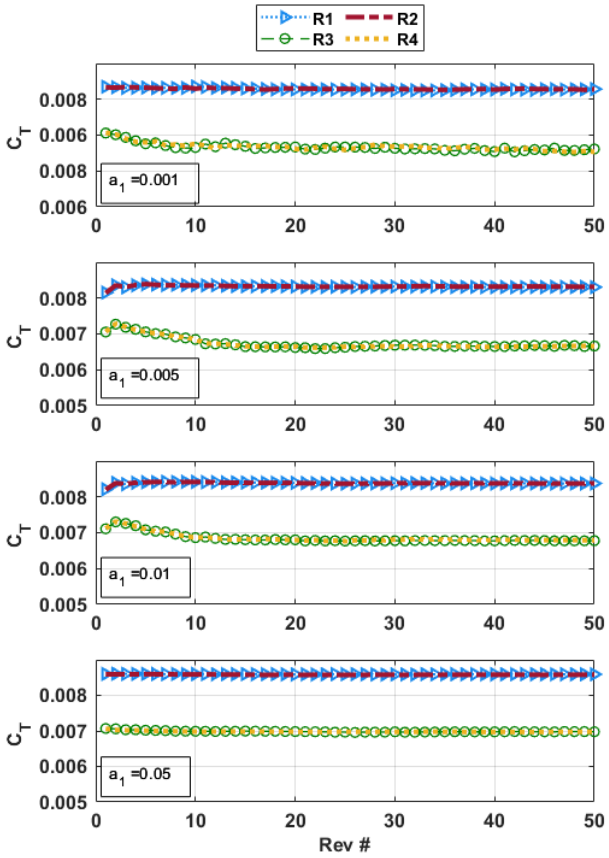

Figure 7. CHARM C_T variation over number of revolutions for each rotor at different diffusion gains: quadrotor at tilt angle of 0 degree and pitch angle of -10 deg, 3000 RPM, 40 ft/s.

Figure 8 and Figure 9 show the side and top view of the visualization of the wake interactions between the fore and aft rotor wakes within the tunnel test section, evaluated at diffusion gain of 0.001, 0.005, 0.01, and 0.05. Table 7 compares the mean absolute discrepancy percentages between the

experimental data and CHARM predictions for C_T values at different diffusion gains of 0.001, 0.005, 0.01, and 0.005. The results suggest that applying a diffusion gain of 0.01 produced the best C_T prediction on average by ∼3.7% for the fore and ∼0.5% for the aft rotors. Therefore, a diffusion gain of 0.01 will be used for the remainder of this study.

Table 7. Rotor 1 and 3 thrust sensitivity to the diffusion gain selected, shown by mean absolute discrepancy percentage in C_T between experimental measurement and CHARM simulation.

Diffusion gain	0.001	0.005	0.01	0.05
Rotor 1	7.97	7.64	4.39	5.57
Rotor 3	6.89	7.14	6.46	9.28

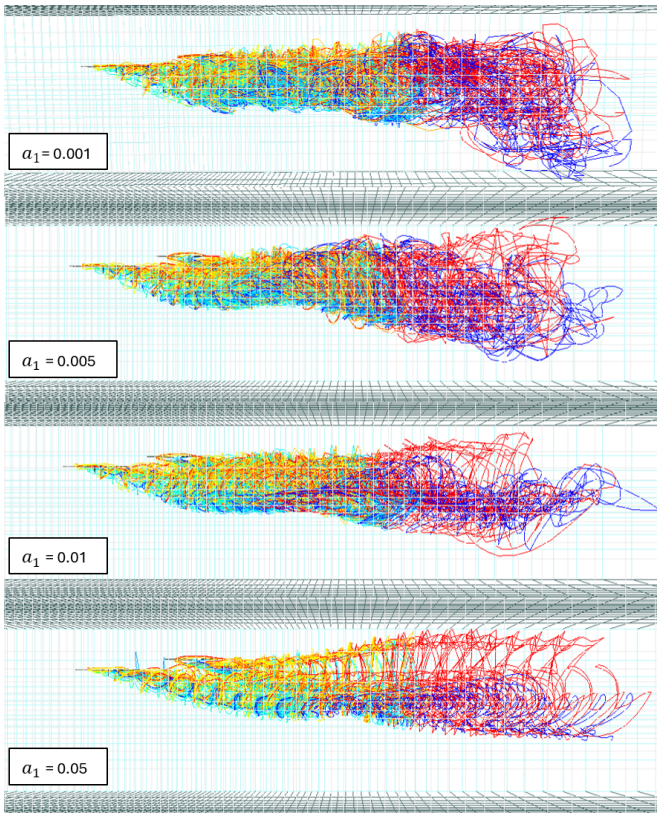

Figure 8. Side view of wake visualization of the quadrotor at a pitch of 0 deg, 3000 RPM, 40 ft/s at various diffusion gains in CHARM.

In CHARM, the blades were modeled using the vortex lattice method. CHARM allows the user to select the number of vortex filaments and the number of vortex elements (BCVE's) along each filament to use in the CVC wake model. The fourth parameter that was selected for the sensitivity study is the number of full-span wakes along the rotor blades, where each blade was modeled with a single row of 80 equal-spaced vortex lattice, and 20 vortex filaments released from the full span of each rotor blade of the quadrotor model. For this sensitivity study, the wake was modeled with 8, 10, and 15 turns of full-span wake followed by 8, 20, and 50 turns of single-tip filament wake, respectively, for three cases of sensitivity study.

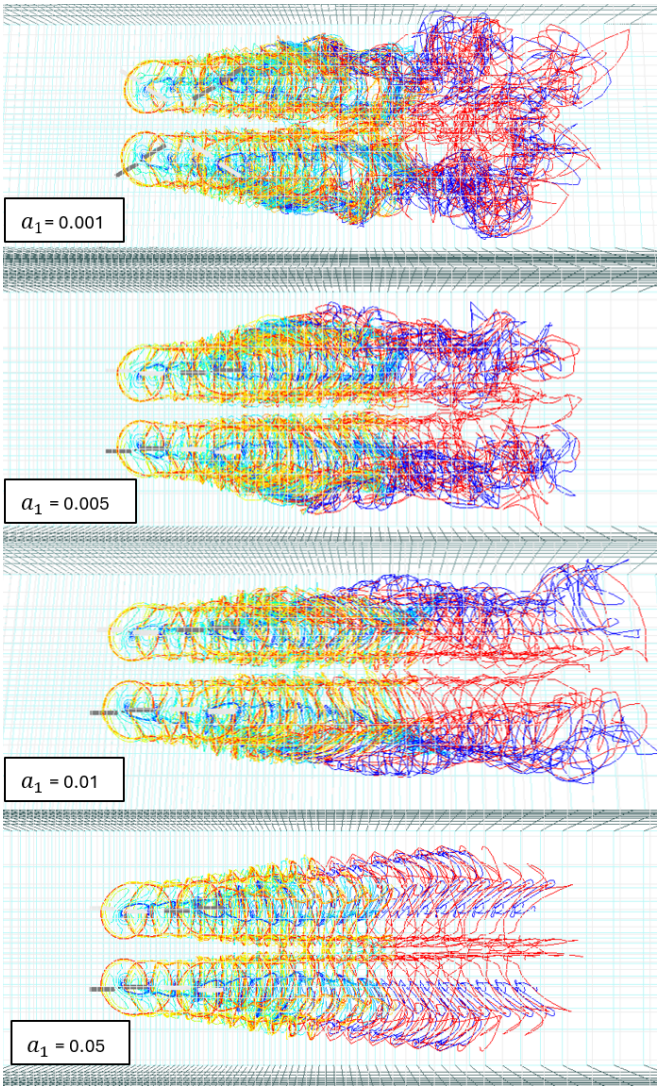

Figure 9. Top view of wake visualization of the quadrotor at a pitch of 0 deg, 3000 RPM, 40 ft/s at various diffusion gains in CHARM.

Table 8 shows the comparison of the mean absolute discrepancy percentages derived from the experimental data in relation to the CHARM predictions for the full-span wake numbers sensitivity study.

Table 8. Rotors 1 and 3 sensitivity to the number of full-span wake turns selected, shown by mean absolute discrepancy percentage in C_T between experimental measurement and CHARM simulation.

# of full-span wake turns	8	20	50
Rotor 1	4.49	4.49	4.46
Rotor 3	6.53	6.76	6.91

The findings reveal that the mean absolute discrepancy percentages produced the same performance results. Since the results show that the fourth case study with the 50 filament wake at the tip took 4 hours to complete, consequently, the remaining simulations presented in this paper will adopt an eight-filament wake at the tip configuration, which significantly reduces the computation time to 1.5 hours.

A total of 100 revolutions were utilized to assess rotor wake interactions in all CHARM computations discussed later in this paper. The wake was modeled using a full-span wake that extended for 8 turns, followed by an 8-turn single tip filament wake within the wind tunnel test section. The tunnel walls were represented using 6,800 panels, with a concentration of panels specifically designed to enhance detail in the central region of the test section.

OVERFLOW Sensitivity Study for the Quadrotor

The aim of this subsection was to perform a sensitivity study for modeling rotor-rotor interference within the context of mid-fidelity BET-based OVERFLOW CFD simulations. To accomplish this, a simplified, inviscid wall-based wind tunnel representation was used, and all rotors were modeled with BET disk modeling. Before this research, a preliminary sensitivity analysis was performed to identify a suitable baseline case and key parameters of interest for variation. The established baseline case featured a grid spacing of 50% chord length for the uniform refinement box, utilized a laminar model (no turbulence model), and employed 4^{th}-order accurate spatial discretization of the Euler terms. From this baseline, three modeling parameters were independently varied to evaluate their sensitivity on the simulation outcome. Namely, the parameters of interest for variation were background grid resolution, solver turbulence model, and accuracy of the central differencing-based spatial discretization of the Euler terms. A summary of each varied parameter is provided in Table 9. Since the focus is mid-fidelity CFD simulation, this sensitivity study prioritizes two factors: solution accuracy and the computational cost of executing the CFD simulation.

Table 9. Simulation variables for sensitivity analysis in predicting rotor aerodynamic performance of quadrotor systems using OVERFLOW.

Parameter	Values
Background grid resolution	50%c, 25%c, 12.5%c
Turbulence model	Laminar, S-A, K-ω
Order of spatial differencing	2^{nd}, 4^{th}, 6^{th}

This study first independently varied the background mesh refinement. The background mesh refinement was increased by reducing the node spacing in the uniform refinement area from 50% chord to 25% chord and then to 12.5% chord length. Results in Figure 10 illustrate that rotor-rotor wake interactions visually increase as refinement progresses from 50% chord to 12.5% chord. In Figure 10, the rotor wake for the 50% chord refinement case is shown to defuse more quickly compared to the 12.5% chord refinement case, leading to weaker interactions among wakes as the wake travels downstream. However, despite these significant differences in downstream wake predictions, boosting background mesh refinement minimally influences the thrust predictions when averaged across all 10 quadrotor CFD simulations. Table 10 summarizes the mean absolute discrepancy percentage in CFD thrust prediction against experimental data, clearly indicating that even with background mesh refinement increased by a factor of 4, the mean absolute discrepancy changes by less than a quarter percentage point. Nevertheless, this fourfold increase in mesh refinement brings about a marked increase in computational cost. For instance, simulating with a 50% chord length refinement takes 10 minutes on 84 CPUs, while simulating with a 12.5% chord length refinement requires 2 hours on 168 CPUs. Evidence from this study suggests that to accurately capture rotor-rotor interference in mid-fidelity BET modeling, using a coarse background mesh greatly minimizes overall computational costs while preserving an adequate level of fidelity. However, it is noted that in coarsening the background mesh, it is essential to ensure sufficient overlap between the background and rotor disk is retained such that orphan points are minimized when oversetting.

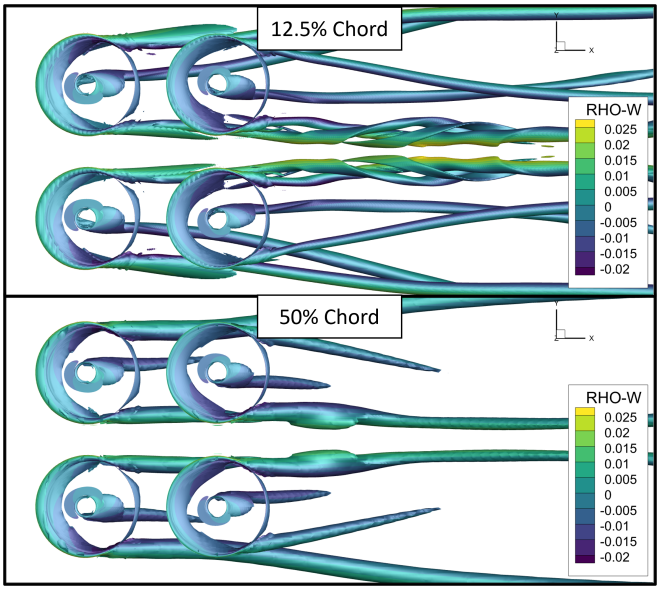

Figure 10. Top down visualization of predicted quadrotor wakes for chord refinement study. Graphic shows iso-surfaces of q-criterion contoured by normalized z-axis momentum.

The second parameter explored in this study was the turbulence model employed. For this parameter sweep, three turbulence modeling approaches were selected: Laminar (no turbulence model), Spalart-Allmaras single-equation model (S-A), and Wilcox's 2006 two-equation model (k-ω). The findings of this sensitivity analysis are summarized in Table 11. The results indicate that, for the configuration examined, the choice of turbulence model has only a minimal impact on the thrust coefficient. When comparing the selected turbulence models,

Table 10. Rotors 1 and 3 sensitivity to background refinement, shown by mean absolute discrepancy percentage in C_T between experimental measurement and OVERFLOW simulation.

Background Refinement	50%c	25%c	12.5%c
Rotor 1	5.078	5.068	5.115
Rotor 3	10.132	10.032	10.032

the mean absolute prediction discrepancy in thrust coefficient varied by just 1% for both the fore and aft rotors. Among the models analyzed, the k-ω model on average provided a small, yet measureable, accuracy improvement in relation to experimental measurements, yielding approximately a 1% enhancement in thrust coefficient predictions for the fore rotor when compared to the Laminar model. Furthermore, compared to the S-A model, the k-ω model demonstrates a similar 1% improvement in thrust predictions for the aft rotor. Given that all three modeling approaches entail a comparable computational cost, the study identifies the k-ω model as the most effective choice for the current configuration.

Table 11. Rotors 1 and 3 sensitivity to turbulence model selected, shown by mean absolute discrepancy percentage in C_T between experimental measurement and OVERFLOW simulation.

Turbulence Model	Laminar	S-A	k-ω
Rotor 1	5.078	4.399	4.008
Rotor 3	10.132	9.911	9.104

The final parameter examined in this study was the order accuracy of the spatial differencing. For this parameter sweep, three order accuracy schemes were selected: 2nd, 4th, and 6th order schemes, Table 12.

Table 12. Rotors 1 and 3 sensitivity to order accuracy of central differencing, shown by the mean absolute percent discrepancy in C_T between experimental measurement and OVERFLOW simulation.

Order	2^{nd}	4^{th}	6^{th}
Rotor 1	6.849	4.766	4.103
Rotor 3	8.809	9.745	12.519

Among all the parameters varied in this study, the thrust coefficient exhibited the greatest sensitivity to the order accuracy parameter. Additionally, it was uncertain which order of accuracy yielded the optimal solution. Transitioning from 2nd to 6th order accuracy resulted in an approximate 4% decrease in the mean absolute discrepancy of the predicted thrust coefficient for the fore rotors, while for the aft rotors, the discrepancy increased by roughly 4%. The results from this parameter sweep also appear to contradict findings from the background grid refinement study. While thrust coefficients demonstrated considerable sensitivity to the chosen discretization order accuracy, the predictions of thrust coefficients remained largely unchanged when varying the background grid refinement.

Although further investigation is needed, the results presented in this section suggest that, at least for the configuration analyzed in this study, the predicted thrust coefficients may be more closely correlated with the near-body rotor grids than with background grid refinement. Given the large sensitivity of rotor thrust predictions to the selected discretization accuracy, it is clear best practices were not identified in this study for the order accuracy parameter. More work is required to confirm or disprove the studies current hypothesis and to outline best practices for future simulations. In the absence of said future validation work, for the remainder of the simulations conducted in this study, it was concluded that the OVERFLOW default 4th order accuracy spatial difference scheme would be used.

COMPARING COMPUTATIONAL PREDICTION WITH AERODYNAMICS EXPERIMENTAL DATA

Using the lessons learned from sensitivity study sections for CHARM and OVERFLOW, the rotor aerodynamic performance was computed for conceptual quadrotor, tandem, and single rotor configurations. For clarity, the MTB2 model is a scaled down version of the conceptual quadrotor reference vehicle. Due to limitations in lateral and longitudinal spacing for the MTB2 test bed, the lateral and longitudinal rotor spacing capabilities enable a close approximation to the rotor spacing of the conceptual quadrotor reference vehicle. For this reason, the rotor positions simulated match the rotor positions utilized in the MTB2 experiment. Figure 11 shows the top view of the rotors inside the test section, with the rotor numbers, spin directions, wind direction, and location of each rotor with respect to the wind tunnel walls presented.

The fore rotor is at a tilt and pitch angle of 0 degrees and is located at a height of 4.77 ft from the wind tunnel floor, with a height difference between the fore and aft rotors of 0.33 ft. All simulations were completed by replicating the corresponding test condition for each data point, including wind tunnel speed and air density. Each resulting simulation point presented is an average of over last 30 revolutions for CHARM and the last 500 iterations for CFD, primarily to improve the prediction comparison with measurements by mitigating the effects of the unsteady solution.

Conceptual Quadrotor Configurations in Forward Flight

The simulations were performed for four 2-bladed MTB2 rotors in the conceptual quadrotor configuration, at forward flight speeds of 20 ft/s and 40 ft/s, RPMs of 2000 and 3000, a rotor tilt of 0 degrees, and model pitch angles of 0, -5, and -10 degrees. Figure 12 and Figure 13 show the computed rotor-wake interactions between the fore and aft rotors at 2000 RPM and 40 ft/s from CHARM and OVERFLOW, respectively.

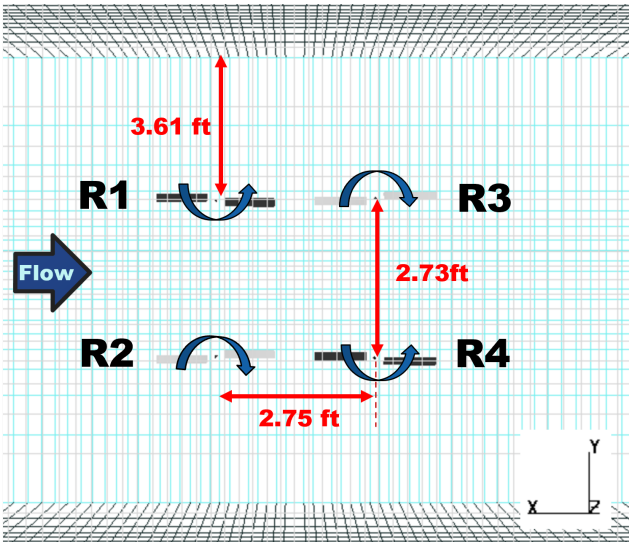

Figure 11. Top view showing rotor locations inside the wind tunnel boundary for the quadrotor configuration at 0 degree tilt and pitch angle in simulations.

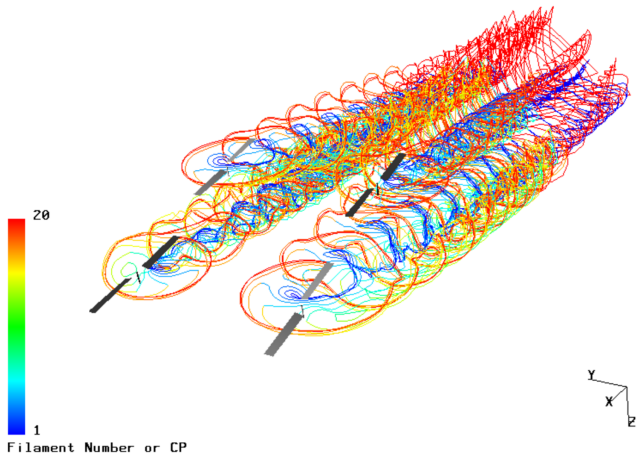

Figure 12. CHARM wake visualization of the conceptual quadrotor configuration at a pitch of -10 deg, 40 ft/s, and 2000 RPM.

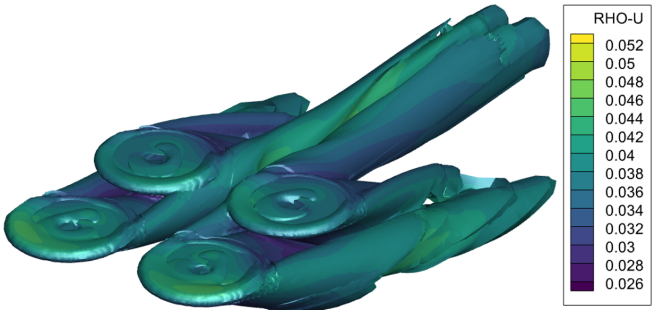

Figure 13. OVERFLOW vorticity isosurface for the conceptual quadrotor configuration at a pitch of -10 deg, 40 ft/s, and 2000 RPM.

Experimental data was anticipated to reveal comparable performance between the fore rotors (Rotor#1 and Rotor#2), as they will encounter the incoming flow with minimal interference from the test stand structure and the wake from other rotors. Likewise, the performance of the aft rotors (Rotor#3 and Rotor#4) was expected to be consistent and comparable. It is important to note that the aft rotors are projected to exhibit a lower thrust coefficient (C_T) compared to the fore rotors. This variation is attributed to the wake interactions caused by the fore rotors and the associated shedding effects from the test stand structure, which would influence the experimental data for the aft rotors.

The comparison between the experimental data and computational predictions from CFD (disk modeling) and CHARM (Blade Element) are shown in Figure 14 and Figure 15 at pitch angles of 0, -5, and -10 degrees for corresponding forward flight speeds of 20.3, 20.3, and 20.1 ft/s (matching tunnel conditions from the run point) at 2000 RPM for the fore rotors and aft rotors).

The comparison between the experimental data and computational predictions from CFD (disk modeling) and CHARM (Blade Element) are shown in Figure 14 and Figure 15 at pitch angles of 0, -5, and -10 degrees for corresponding forward flight speeds of 20.3, 20.3, and 20.1 ft/s (matching tunnel conditions from the run point) at 2000 RPM for the fore rotors and aft rotors). Since the computational values for both port and starboard side rotors were almost equal, only computed predictions for Rotor#1 and Rotor#3 are shown from CHARM and CFD.

Both the experimental data and the simulation results show an increase in C_T for increasing pitch angle for the fore and aft rotors. Figure 14, shows CHARM results differ from experimental C_T values by 3.4-7.5% for the fore rotors and within 3.8-11.2% for the aft rotors, while the CFD results differ from experimental C_T values by 1.5-10.4% for fore rotors and within 0.9-7.5% for aft rotors. The discrepancy percentage values are for across the different pitch values and comparing both to Rotor#1 and Rotor#2 experimental values.

Similarly, Figure 16 and Figure 17 show a comparison of experimental and simulation predictions for 3000 RPM and wind speeds of 40.5, 40.4, and 40.4 ft/s for the fore and aft rotors at pitch angles of 0, -5, and -10 degrees, respectively. These results indicate that simulation software predicts similar C_T values for the fore and aft rotors. However, the experimental data show C_T values for the fore rotors that are 4.0-10.3% higher than the CHARM predicted values and 3.8-9.3% higher than the CFD predicted values. Figure 17 shows lower C_T experimental values for aft rotors at pitch angle of 0 degree which could be due to an increase of wake on wake interactions at higher velocities and RPMs. CHARM predicted the C_T values for Rotor#3 within 3.1-8.5%, and CFD within 3.3-10.2%. Also, Figure 17 shows asymmetry in experimental data for Rotor#3 and Rotor#4. It was expected that Rotor#4 and Rotor#3 would have similar C_T values since the MTB stand is symmetrical, and the two aft rotors should encounter similar flow conditions.

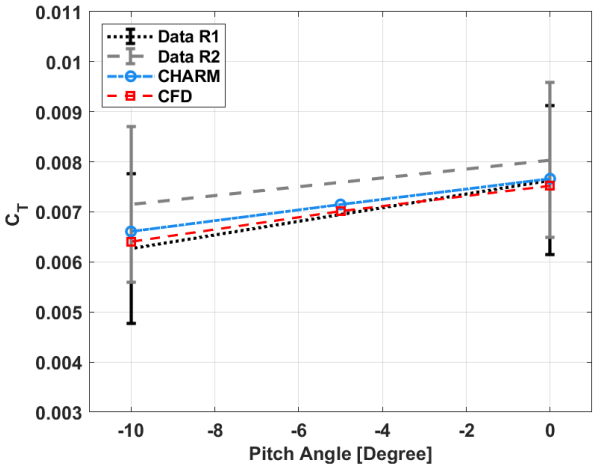

Figure 14. Conceptual quadrotor thrust comparison for the fore rotors at 2000 RPM and tunnel speed of ∼20 ft/s (μ= 0.093).

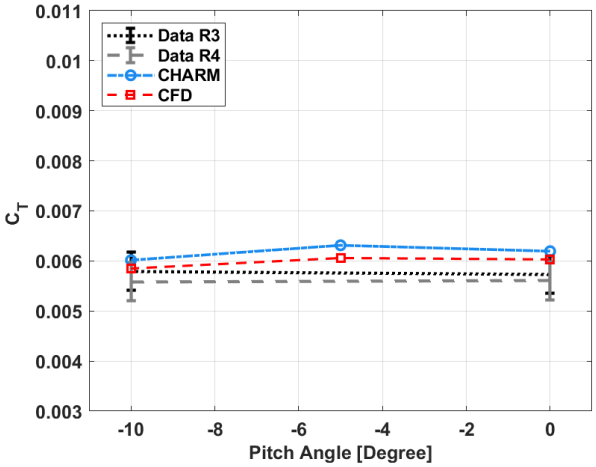

Figure 15. Conceptual quadrotor thrust comparison for the aft rotors at 2000 RPM and tunnel speed of ∼20 ft/s (μ= 0.093).

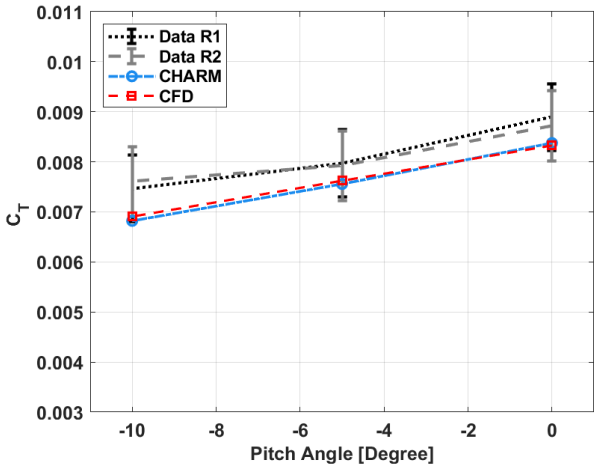

Figure 16. Conceptual quadrotor thrust comparison for the fore rotors at 3000 RPM and tunnel speed of ∼40 ft/s (μ=0.124).

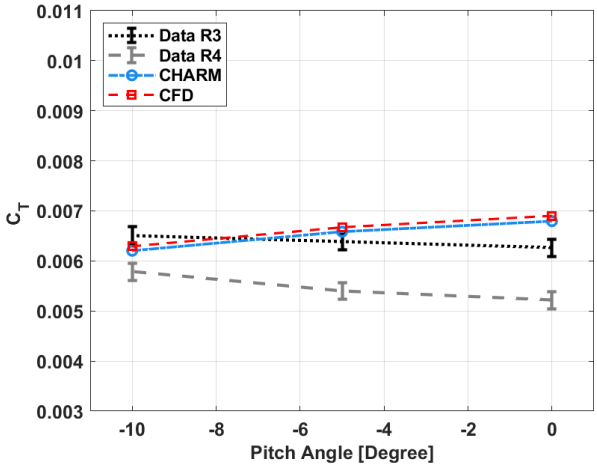

Figure 17. Conceptual quadrotor thrust comparison for the aft rotors at 3000 RPM and tunnel speed of ∼40 ft/s (μ= 0.124).

One of the goals of this study is to provide recommendations for MTB3, so this section will briefly discuss possible sources of error. The observed discrepancies between the starboard and port side rotors may be attributed to dynamic load variations experienced by the load cells, which impact the average values recorded for each data point. Studying the dynamic data for the fore load cells could provide insight into the source of error, which is outside the scope of this study, (Ref. 21). Also, dynamic data of the wind tunnel conditions were not recorded, and only the recorded average wind tunnel speed was used for the simulations. This finding can be consider when assessing the MTB3 testing campaign.

Asymmetry in the wind tunnel flow could also cause observed differences between the starboard and port rotors. However, the asymmetry in the wind tunnel flow is unlikely to contribute to the differences observed between the starboard and port rotors, as flow quality studies conducted in the U.S. Army 7- by 10-Foot Wind Tunnel have consistently produced favorable results (Ref. 22). Additionally, the differences in rotor performance could stem from small variations between the individual manufactured blades. An imbalance in the rotor blades may also adversely affect the performance of both port and starboard rotors.

Further, discrepancies in simulated and experimental performance predictions may stem from inaccuracies within the 2D aerodynamic coefficients provided in the airfoil tables. The airfoil tables, as mentioned in the MTB2 Reference Blade section, were generated using AFTGen with OVERFLOW to streamline airfoil table generation, but there are limitations when coupled with OVERFLOW. It's possible that a different numerical scheme unavailable in AFTGen with OVERFLOW could improve comparisons of simulation results with experimental data, especially within the Reynolds number range experienced during testing, (Ref. 23).

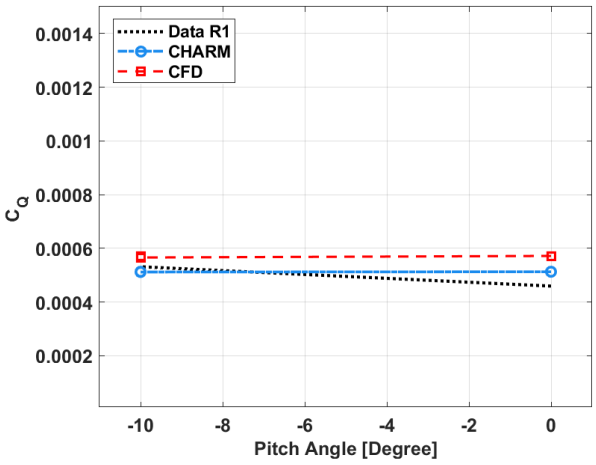

Figure 18. Conceptual quadrotor power predictions comparison for Rotor#1 at 2000 RPM and tunnel speed of ∼20 ft/s (μ=0.093).

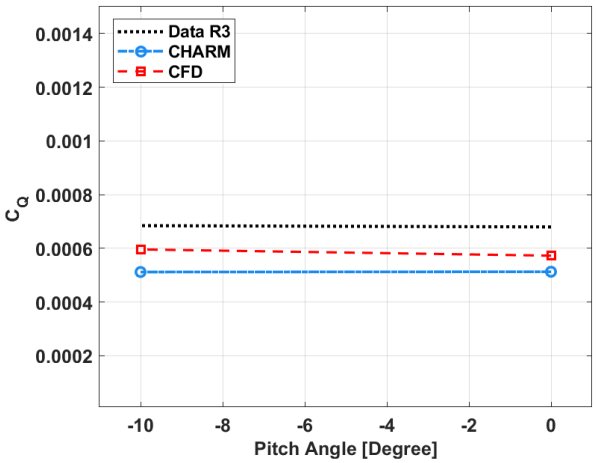

Figure 19. Conceptual quadrotor power predictions comparison for Rotor#3 at 2000 RPM and tunnel speed of ∼20 ft/s (μ=0.093).

In addition, AFTGen does not currently enable low-Mach preconditioning for Mach numbers below 0.2 (a capability currently available in the OVERFLOW solver). Investigating both of these areas could improve simulation results and be accounted for in the generation of MTB3 airfoil tables. Another source of error could be thermal noise, which cannot be verified due to missing thermocouple data. This information can be utilized in discussions surrounding the MTB3 testing campaign. To investigate the source of error further, results from single rotor and tandem cases can be analyzed to identify other variables influencing the observed asymmetry. For additional comparison of conceptual quadrotor experimental and simulation results, please refer to Appendix A, which includes data for operations at 2000 RPM with a forward velocity of 40 ft/s, as well as for 3000 RPM at a forward velocity of 20 ft/s.

In order to compare the power directly, the rotors were

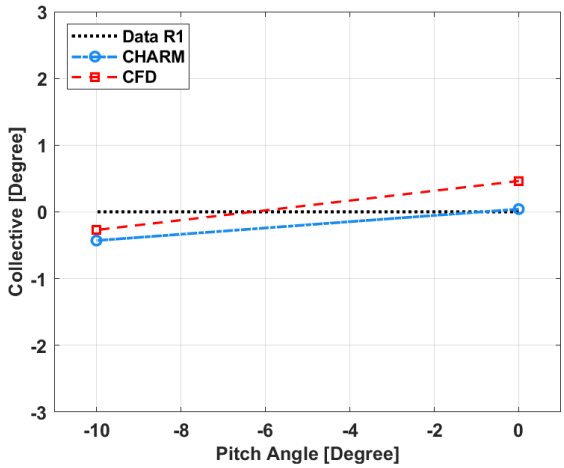

Figure 20. Conceptual quadrotor collective prediction comparison for Rotor#1 at 2000 RPM and tunnel speed of ∼20 ft/s (μ= 0.124).

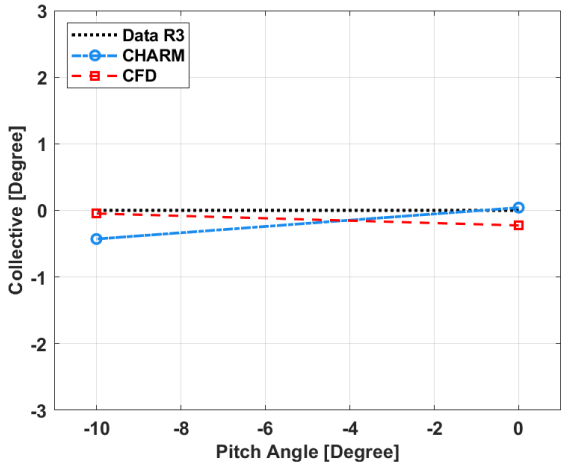

Figure 21. Conceptual quadrotor collective prediction comparison for Rotor#3 at 2000 RPM and tunnel speed of ∼20 ft/s (μ= 0.124).

trimmed to the measured thrust values by providing the final C_T values for simulations and allowing collective to be adjusted.

Figure 18 and Figure 19 show the CHARM and CFD C_Q prediction values for the quadrotor for different pitch angles at RPM of 2000 at forward flight speed of 20 ft/s for Rotor#1 and Rotor#3, respectively. The corresponding collective predictions were presented in Figure 20 and Figure 21. These results indicated that aft rotors generate less thrust due to the downwash from the fore rotors while requiring more power due to the change of induced velocity from the fore rotors and change in thrust values. Similarly the CHARM and CFD C_Q predictions for the quadrotor at RPM of 3000 at forward flight speed of 40 ft/s versus Rotor#1 and Rotor#3 were shown in Figure 22 and Figure 23 with corresponding adjusted collective angle shown in Figure 24 and Figure 25, respectively.

These results show that CHARM and CFD over-predict the

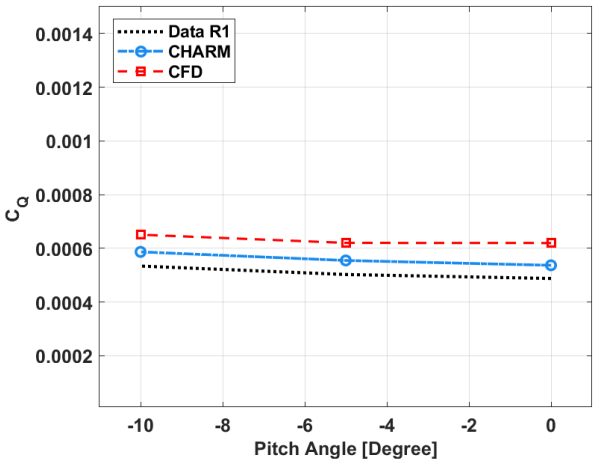

Figure 22. Conceptual quadrotor power predictions comparison for Rotor#1 at 3000 RPM and tunnel speed of ∼40 ft/s (μ= 0.124).

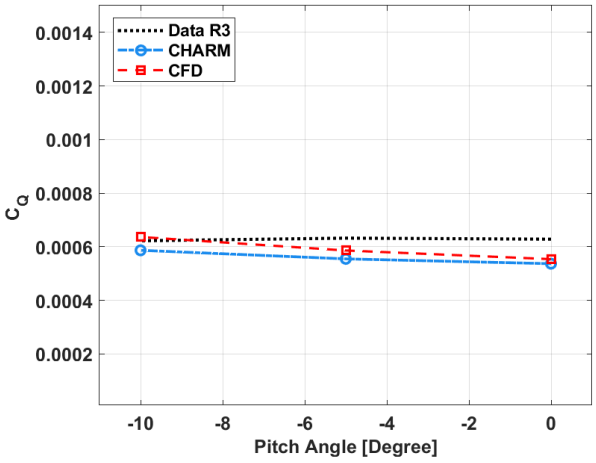

Figure 23. Conceptual quadrotor power prediction comparison for Rotor#3 at 3000 RPM and tunnel speed of ∼40 ft/s (μ= 0.124).

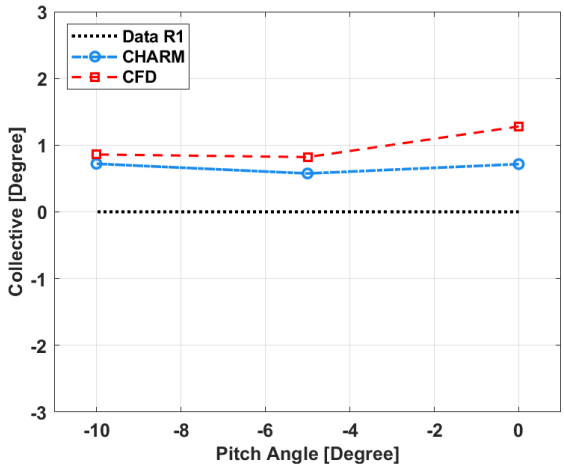

Figure 24. Conceptual quadrotor collective prediction comparison for Rotor#1 at 3000 RPM and tunnel speed of ∼40 ft/s (μ= 0.124).

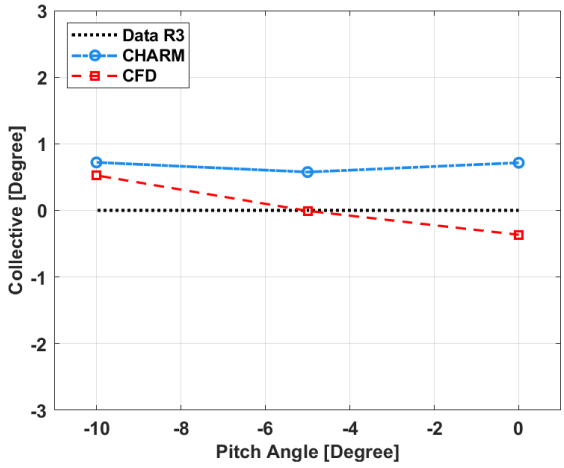

Figure 25. Conceptual quadrotor collective prediction comparison for Rotor#3 at 3000 RPM and tunnel speed of ∼40 ft/s (μ= 0.124).

C_Q value for the fore rotors while under-predicting it for aft rotors at pitch angles of –5 and 0 degrees. Additionally, the findings suggest that at a pitch angle of 0 degrees, producing more thrust than the -10 and -5 degree configurations while requiring a similar amount of power. The simulation predictions trends also aligned with the experimental data trend for C_Q values. Figure 26 and Figure 27 show the contour induced velocity plot for the quadrotor case using OVERFLOW and CHARM at 3000 RPM and the wind tunnel speed of 40 ft/s at pitch angles of 0 and -5 degrees. BET disk models are not intended to provide a realistic and detailed representation of the rotor's wake. Instead, the disk model aims to offer, at best, a time-averaged wake representation. Consequently, there are several differences to expect when comparing the induced velocities observed in CHARM and OVERFLOW. Since the BET disk model applies source terms to the full disk at each iteration, no blade tip vortices are generated. Results presented in this study indicate a significant upwash predicted near the rotor tip in the upwind section of the disk, which is absent when running CHARM. Additionally, near the rotor tip on the advancing side, BET disk modeling consistently predicts more induced velocity compared to CHARM simulations.

This overestimation may result from a magnified depiction of the rotor wake roll-up when using a BET disk model in forward flight, although further research is necessary.

Single Rotor in Forward Flight

During the MTB2 wind tunnel test, each of the four MTB rotors was individually tested in a single rotor case to assess potential variations related to rotor positioning and to identify any discrepancies in load cell readings. The single rotor simulations were performed for each of the four 2-bladed MTB2

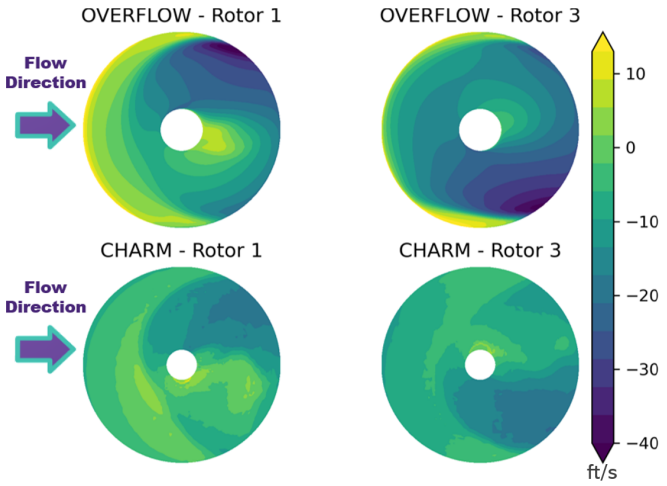

Figure 26. Contour plot of induced velocity for the quadrotor case using OVERFLOW and CHARM at 3000 RPM and wind tunnel speed of 40 ft/s at pitch angle of 0 degree.

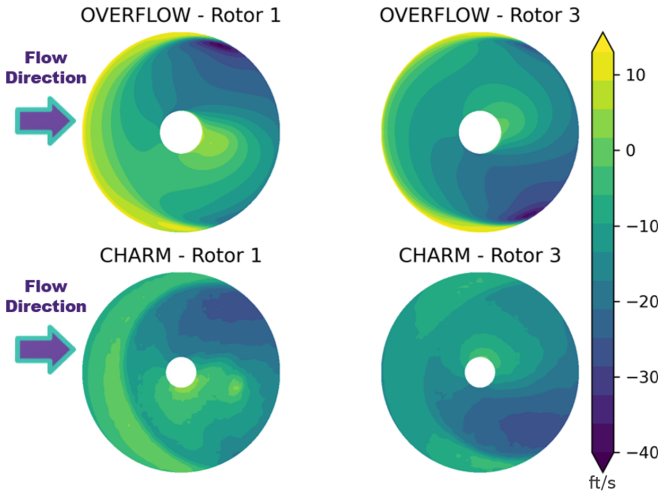

Figure 27. Contour plot of induced velocity for the quadrotor case using OVERFLOW and CHARM at 3000 RPM and wind tunnel speed of 40 ft/s at pitch angle of -5 degree.

rotors in conceptual quadrotor configuration at forward flight speeds of 20 ft/s and 40 ft/s, RPMs of 2000 and 3000, with rotor tilt of 0 degree, and a pitch angles of 0, -5, and -10 degrees for all four rotors individually. Figure 28 and Figure 29 show the single MTB2 rotor wake visualization case at 40 ft/s, 0 degree pitch, and 2000 RPM in CHARM and OVERFLOW, respectively. Due to an issue during experimental testing, the wind tunnel conditions for single rotor cases, with the exception of Rotor#1, were not recorded by the data acquisition system. However, handwritten values were recorded by the testing personnel for the wind tunnel conditions, such as wind tunnel speed and temperature. Therefore, the experimental results from Rotor#1 and #3 will be used to identify and study possible asymmetry in wind tunnel flow or dynamic fluctuation in the data while comparing experimental data with simulation predictions.

Figure 30 and Figure 31 show the experimental data for the single Rotor#1 rotor case for pitch angles of 0, -5, and -10 degrees at forward flight speeds of 20.6, 21.2, 20.6 ft/s and 41.3, 41.3, and 41.2 ft/s respectively for 2000 and 3000 RPM. Figure 30 shows that CHARM over-predicts C_T by 9.8% at the 0 degree pitch angle when compared to the experimental data. Conversely, at a pitch angle of -10 degrees, CHARM demonstrates a more accurate prediction, with a marginal discrepancy of just 4.1%. OVERFLOW, with the disk rotor model, over-predicts the C_T compared to experimental data by 1.6% for a pitch angle of -10 degrees and by 6.6% for the 0 degree pitch angle. At 0 degree pitch for Rotor#1, both simulations over-predict the C_T, unlike for the quadrotor case at 2000 RPM and ∼20 ft/s, which could be an indicator of existing, dynamic variation in data. The rotor wake during testing can also result in increases in wind tunnel speed, and this variability could influence experimental and simulated comparisons. Figure 31, similar to Figure 16, shows the experimental C_T values are higher than the simulations prediction while following the same trend for a sweep of the pitch angles.
Additional experimental and simulation comparisons for the

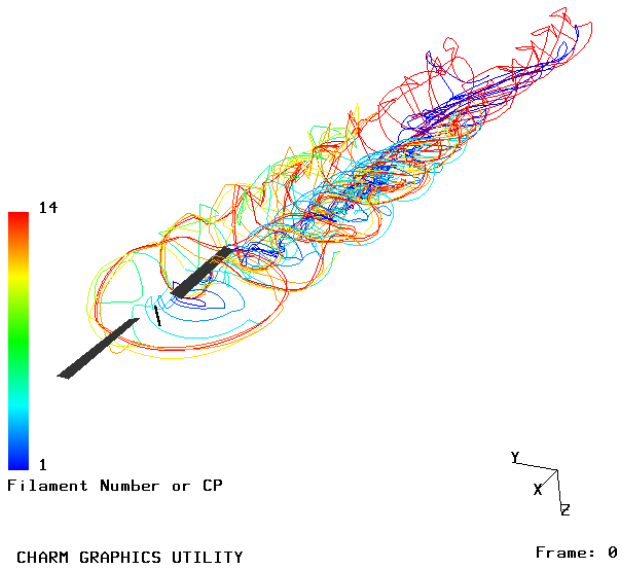

Figure 28. MTB2 rotor wake of the single 2-bladed rotor at 2000 RPM, 0 degree pitch angle, and 40 ft/s wind tunnel speed.

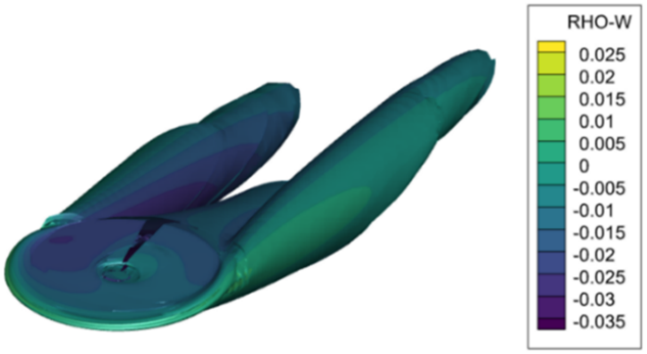

Figure 29. OVERFLOW vorticity isosurface of single MTB2 rotor.

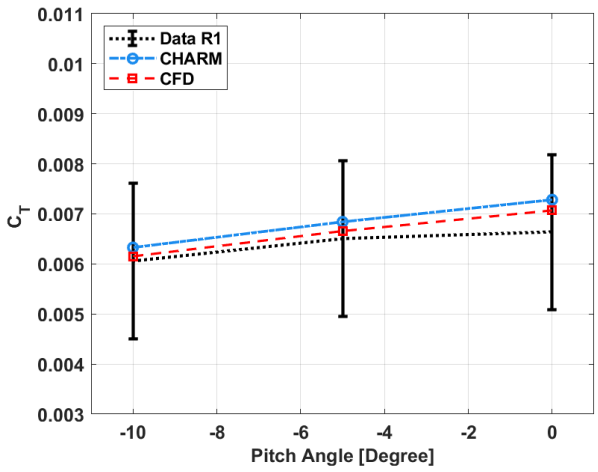

Figure 30. Single rotor thrust comparison at 2000 RPM and tunnel speed of ∼20 ft/s (μ=0.093).

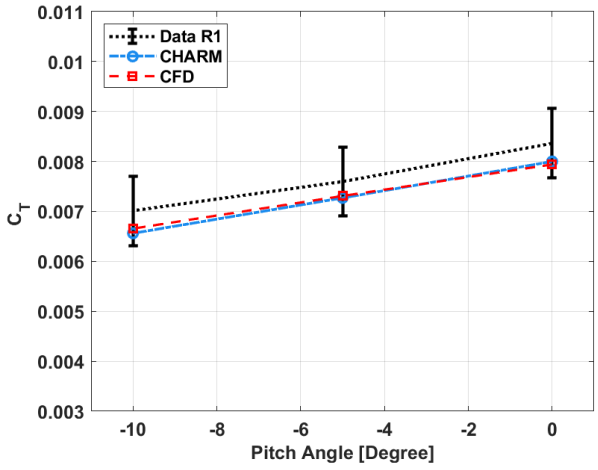

Figure 31. Single rotor thrust comparison at 3000 RPM and tunnel speed of ∼40 ft/s (μ=0.124).

single rotor cases, a combination of 2000 RPM at a forward velocity of 40 ft/s and 3000 RPM at a forward velocity of 20 ft/s, can be found in Appendix B. Comparing the experimental data with the simulation results for Rotor#3 at the wind tunnel speed of 40 ft/s and 3000 RPM shows the contribution of the rotor wake interactions between the fore and aft rotors in the quadrotor cases. Figure 32 shows the experimental data for 3000 RPM at tunnel speeds of 40.02, 40.15, and 40.09 ft/s for pitch angles of 0, -5, and -10 degrees. CHARM and OVERFLOW predict higher C_T compared to the quadrotor experimental data for the aft rotor Rotor#3, which is expected due to wake-on-wake interactions from the fore rotors and reduction to the induced velocity in the aft rotors. Also, it is possible that in the absence of a wake from the fore rotors, less aerodynamic shedding from the MTB structure will be introduced to the aft rotors, resulting in a higher coefficient of thrust. Also, the single rotor case, compared to the quadrotor, does not get exposed to the wake of the side rotors.

To investigate potential uncertainties associated with the consistency of rotor blade manufacturing, the same set of rotor blades was placed on two different load cells during a single rotor test to assess any differences arising from blade set dissimilarity. Table 13 presents the thrust data obtained from the fore starboard side load cell (R1) and compares it to a scenario where the aft-port side rotor blades (R4) were positioned on load cell R1. The two cases indicate negligible thrust variance, with a minimum of 0.08 lb and a maximum of 0.15 lb. For better comparison, the thrust predictions from simulations for Rotor#1 are presented in Table 13, which indicates a discrepancy of 0.0-6.8% compared to the Rotor#1 ($R1$) experimental data. This experimental data shows that the consistency of rotor blade manufacturing from rotor blade set Rotor#1 has a minor impact on the quality of the data.

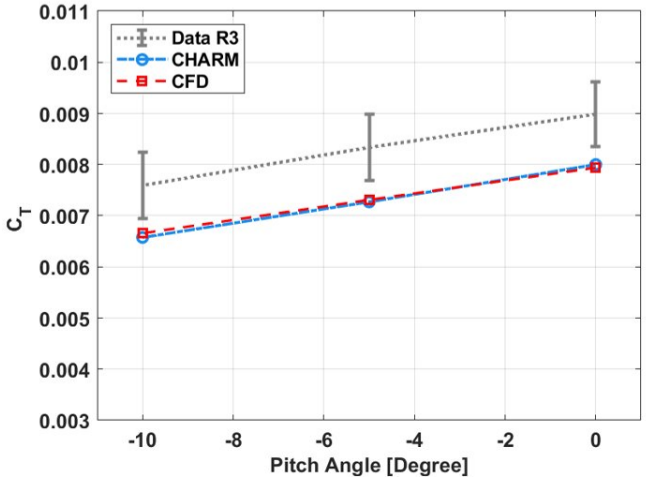

Figure 32. Single rotor thrust comparison at 3000 RPM and tunnel speed of ∼40 ft/s (μ=0.124)) for Rotor#3.

Table 13. MTB2 thrust data from the single load cell, fore-starboard rotor, and the different in performance with different sets of blades at 2000 RPM and tunnel speed of ∼40 ft/s.

	Pitch [°]		
Thrust [lb]	0	-5	-10
R1	3.1	2.7	2.3
CHARM	3.2	2.7	2.3
CFD	3.2	2.9	2.5
Δ Thrust [a]	0.08	0.09	0.11

[a]The aft-port rotor blade set placed on load cell R1 and compared to original R1 case experimental data

Tandem Configurations in Forward Flight

The study of the tandem rotor configuration provides valuable insights into the effects of rotor wake interactions from the fore rotors, independent of the influence exerted by side rotors. This approach facilitates a more precise comparison of the starboard-side rotors (Rotor#1, Rotor#3) in isolation from the port side counterparts. Two 2-bladed rotors were modeled

in the U.S. Army 7- by 10-Foot Wind Tunnel test section at 2000 RPM for pitch angles of 0, -5, and -10 degrees at tunnel speeds of 20.2, 20.2, and 20.4, shown in Figures 33-34. Both CHARM and OVERFLOW under-predict the fore rotor C_T. CHARM exhibited a discrepancy range of 3.4-6.1%, while CFD exhibited a discrepancy range of 5.7-9.7% for the fore rotor; however, for the aft rotor, CHARM predicted the C_T within 1.7-5.1% of experimental data, while CFD predictions were within 0.0-3.3% of the experimental data.

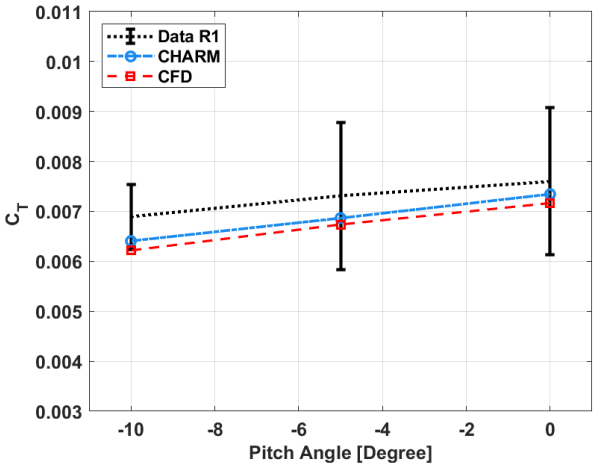

Figure 33. Tandem thrust comparison for the fore rotor at 2000 RPM and tunnel speed of ∼20 ft/s (μ= 0.093).

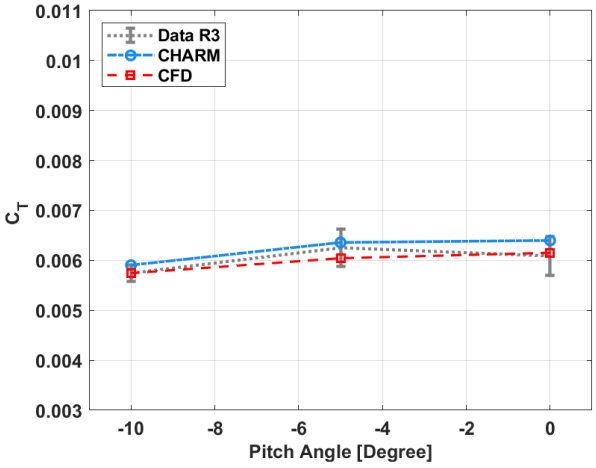

Figure 34. Tandem thrust comparison for the aft rotor at 2000 RPM and tunnel speed of ∼20 ft/s (μ= 0.093).

Figures 35-36 illustrate the experimental data collected at 3000 RPM and approximately 40 ft/s during the pitch angle sweep. For the fore rotor, both CHARM and CFD exhibit a similar under-prediction ranging from 9.8% to 13.8% of the experimental C_T values. In contrast, both methods accurately capture the C_T values for the aft rotor, with CHARM showing a discrepancy of 1.69% to 6.3% and CFD demonstrating a discrepancy of 2.8% to 4.1%. Additional experimental and simulation comparisons for the configurations of 2000 RPM at a forward velocity of 40 ft/s and 3000 RPM at 20 ft/s can be found in Appendix C.

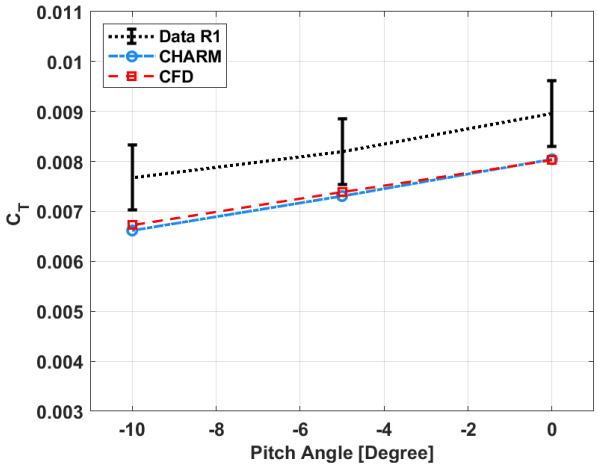

Figure 35. Tandem thrust comparison for the fore rotor at 3000 RPM and tunnel speed of ∼40 ft/s (μ= 0.124).

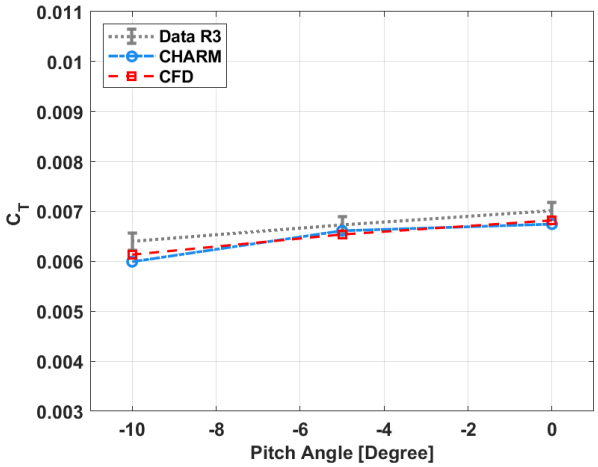

Figure 36. Tandem thrust comparison for the aft rotor at 3000 RPM and tunnel speed of ∼40 ft/s (μ= 0.124).

CONCLUSIONS

One of the objectives of this study was to provide sensitivity analysis in predicting rotor aerodynamic performance using comprehensive analysis for rotor performance prediction and validating tools for Vertical Take-Off and Landing (VTOL) aircraft. This work utilized MTB2 experimental test data to study sensitivity for predicting rotor performance of the quadrotor using two mid-fidelity tools, CHARM and Blade Element Theory (BET) based disk modeling in the OVERFLOW CFD solver. This work provides sensitivity studies for capturing aerodynamic rotor wake interactions for the quadrotor configurations using CHARM and OVERFLOW analyses. The analyses were validated using the MTB2 experimental data for conceptual quadrotor configuration. Table 14 and Table 15 show a summary of input parameters and recommended values for implementation in both CHARM and OVERFLOW for the quadrotor configuration. These findings aim to enhance the accuracy of aerodynamic predictions for multirotor configurations, providing cost- and time-efficient solutions for VTOL applications.

For OVERFLOW, a simplified inviscid wind tunnel representation was used, with all rotors modeled as BET disks. A preliminary sensitivity study established a baseline case that included a grid spacing of 50% chord length, a K-ω model, and 4th-order accurate spatial discretization of Euler terms, Table 15. For CHARM a total of 100 revolutions were suggested for the quadrotor configurations to evaluate rotor wake interactions. The wake was modeled using a full-span configuration that extended over 8 revolutions followed by an 8-revolution single tip filament wake and diffusion gain of 0.01 within the wind tunnel test section. The tunnel walls were represented using 6,800 panels, with a concentration of panels in the central region of the test section, Table 14.

Table 14. The recommended values for predicting rotor aerodynamic performance of the quadrotor systems using CHARM.

Parameter	Values
Surface panel resolution	6,800
# of revolutions	100
Diffusion gain	0.01
# of full-span wake turns	8

Table 15. The recommended values for predicting rotor aerodynamic performance of the quadrotor systems using OVERFLOW.

Parameter	Values
Background grid resolution	50%c
Turbulence model	K-ω
Order of spatial differencing	4^{th}

The sensitivity studies for the quadrotor cases were utilized to examine experimental data using the single and tandem experimental data. The comparative analysis of the single rotor, tandem, and quadrotor configurations at the forward flight velocity of 40 ft/s and RPM of 3000 indicates that both CHARM and CFD exhibit a consistent under-predict of the thrust coefficient (C_T) values for the fore rotors. One potential factor contributing to this observed trend may be the airfoil tables utilized by both software programs. Note that the existing airfoil tables cover Mach numbers ranging from 0.1 to 0.5 in increments of 0.1, which does not exceed the Mach numbers experienced by the rotor, even at higher RPM and wind tunnel velocities. The 2D aerodynamic coefficients calculated in the airfoil tables utilized AFTGen coupled with OVERFLOW, as described in the MTB2 Reference Blade section. However, there are some limitations within AFTGen that may influence the accuracy of airfoil table calculations, including limited numerical method options and the inability to apply low Mach number preconditioning. Another contributing factor to this trend may be the assumption in both CHARM and OVERFLOW that the rotor blades are rigid, which could lead to discrepancies in performance predictions at higher advance ratios.

Future Work

In order to improve the accuracy of computational predictions and to further investigate parameter sensitivity in upcoming simulations, the following recommendations were suggested:

- Consider re-running cases from Mach 0 to 0.2 in OVERFLOW directly to incorporate low Mach number preconditioning options in 2D airfoil simulations and compare with original AFTGen with OVERFLOW results.
- Investigate the impact of including MTB structure model in both CHARM and OVERFLOW simulations.
- Examine the influence of wall effects in both CHARM and OVERFLOW by comparing simulations conducted in free field conditions with the current results.
- Explore the impact of blade elastic deformations in CHARM and OVERFLOW. Consider repeating the quadrotor simulation study using a nonrigid rotor model. An elastic rotor blade model might improve the rotor performance prediction for MTB2 rotor blade specially at higher wind tunnel speeds and RPMs.
- Investigate the effect of removing a fraction of the inboard wake on the CHARM rotor performance predictions.
- Expand the sensitivity analysis of OVERFLOW to include disk mesh refinement.
- Consider the C_Q in sensitivity studies, particularly in CHARM when changing the diffusion gain value. The wake strength of fore rotors is directly affected by diffusion gain value, and therefore impacts the power prediction of the aft rotors.

This sensitivity study, in conjunction with comparing the MTB2 experimental data and the computational rotor performance predictions, provided insight to identify some suggestions for the future MTB experimental test, MTB3. These suggestions are summarized as follows:

- Consider implementing repeat data points for specific RPM, pitch, and tilt conditions into the test matrix to expand the reach of the sensitivity studies. While expanding the test matrix will incur additional time and costs, the knowledge gained from additional sensitivity studies can help reduce uncertainties and identify error sources in the data.
- Ensure the quality of single-rotor case data. This will help identify discrepancies between the rotors and load cells and any asymmetries in the wind tunnel flow without the presence of rotor-to-rotor interference.
- Conduct tandem configuration tests for Rotor#2 and Rotor#4, in addition to the Rotor#1 and Rotor#3. This will allow for a thorough comparison of rotor wake interactions.

- Ensure that the rotor is balanced to prevent excessive vibrations in the model. This might address discrepancies between the port and starboard rotors.
- Place Resistance Temperature Detectors (RTDs) on each load cell to allow for the identification of any high reading due to thermal noise.

Overall, further investigation is needed to thoroughly analyze the data, execute the CHARM and OVERFLOW simulations, and fully understand the capabilities of both tools to enhance the ability to predict such complex rotor interactions for future MTB tests.

Author contact:

Dorsa Shirazi	dorsa.shirazi@nasa.gov
Nicholas Peters	nicholas.j.peters@nasa.gov
Carl Russell	carl.r.russell@nasa.gov
Sarah Conley	sarah.a.conley@nasa.gov
Kristen Kallstrom	kristen.kallstrom@nasa.gov
Stephen Wright	stephen.j.wright@nasa.gov
Carlos Pereyra	carlos.z.pereyra@nasa.gov
Jordan Mills	millsj25@my.erau.edu

APPENDIX-A

Appendix-A shows additional comparison of conceptual quadrotor experimental and simulation results.

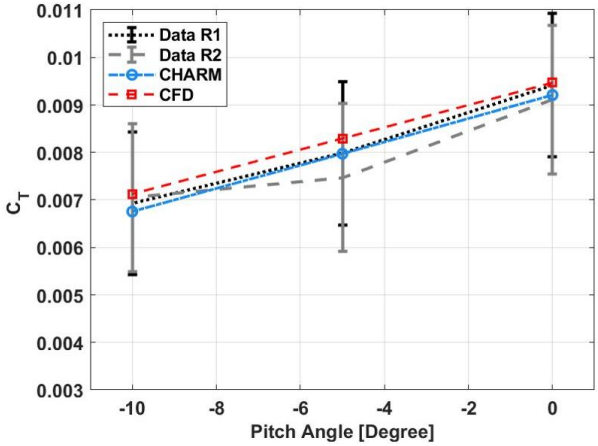

Figure A1. Conceptual quadrotor thrust comparison for the fore rotors at 2000 RPM and tunnel speed of ~40 ft/s.

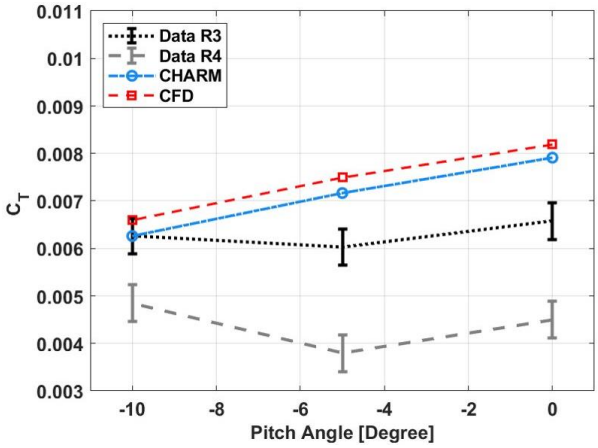

Figure A2. Conceptual quadrotor thrust comparison for the aft rotors at 2000 RPM and tunnel speed of ~40 ft/s.

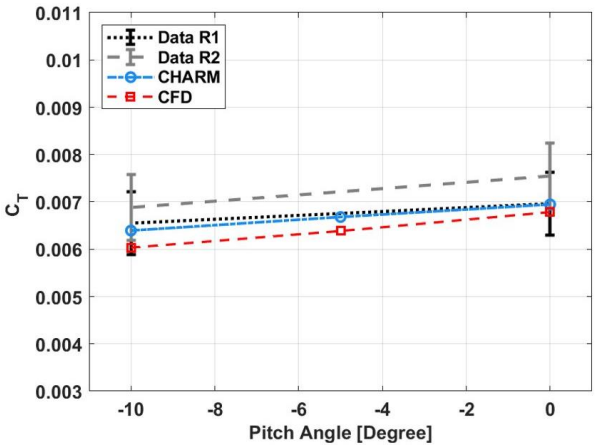

Figure A3. Conceptual quadrotor thrust comparison for the fore rotors at 3000 RPM and tunnel speed of ~20 ft/s.

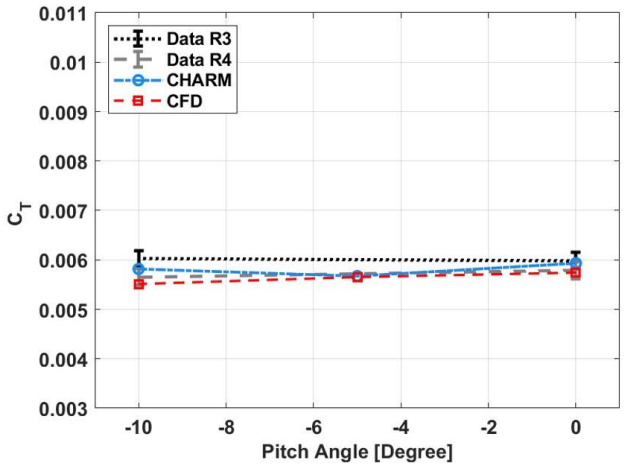

Figure A3. Conceptual quadrotor thrust comparison for the aft rotors at 3000 RPM and tunnel speed of ~20 ft/s.

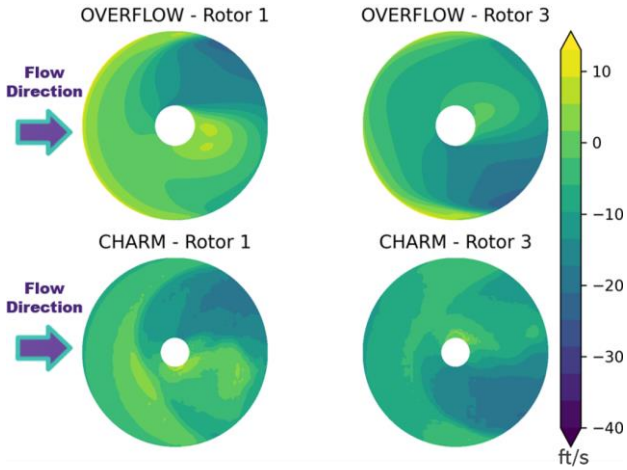

Figure A4. Contour plot of induced velocity for the quadrotor case using OVERFLOW and CHARM at 2000 RPM and wind tunnel speed of 40 ft/s at pitch angle of 0 degree.

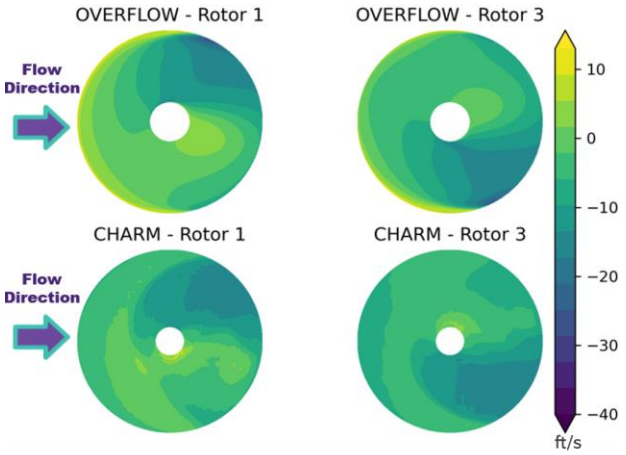

Figure A5. Contour plot of induced velocity for the quadrotor case using OVERFLOW and CHARM at 2000 RPM and wind tunnel speed of 40 ft/s at pitch angle of -5 degree.

APPENDIX-B

Appendix-B shows additional comparison of single rotor experimental and simulation results.

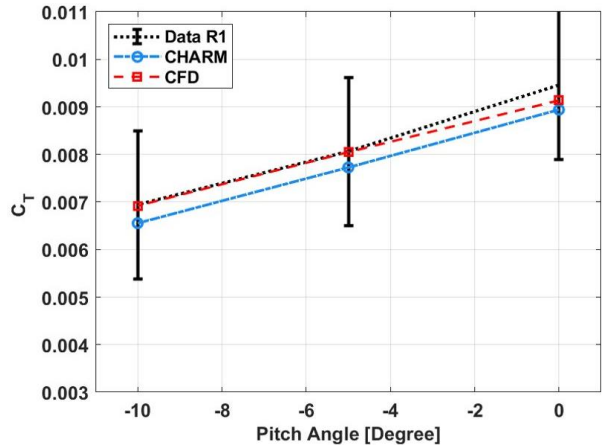

Figure B1. Single rotor thrust comparison at 2000 RPM and tunnel speed of ~40 ft/s (μ=0.185).

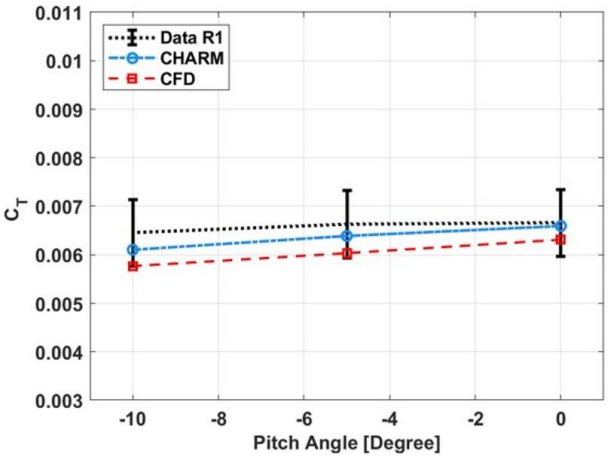

Figure B2. Single rotor thrust comparison at 3000 RPM and tunnel speed of ~20 ft/s (μ =0.062).

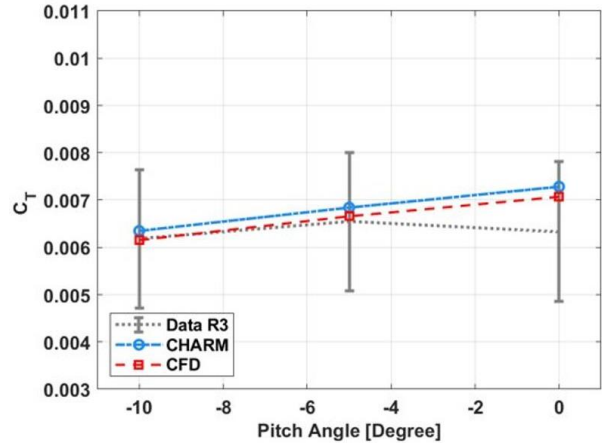

Figure B3. Single rotor thrust comparison at 2000 RPM and tunnel speed of ~20 ft/s (μ =0.093) for Rotor\#3.

APPENDIX-C

Appendix-C shows additional comparison of tandem configuration experimental and simulation results.

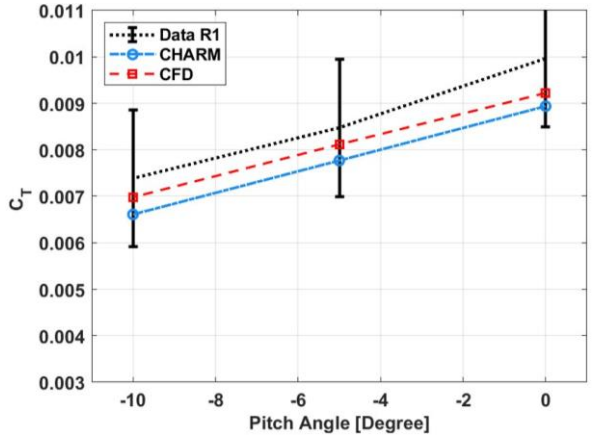

Figure C1. Tandem thrust comparison for the fore rotor at 2000 RPM and tunnel speed of ~40 ft/s (μ = 0.186).

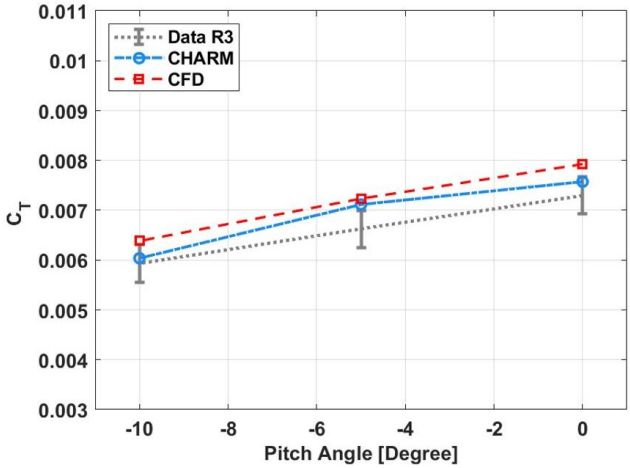

Figure C2. Tandem thrust comparison for the aft rotor at 2000 RPM and tunnel speed of ~40 ft/s (μ = 0.186).

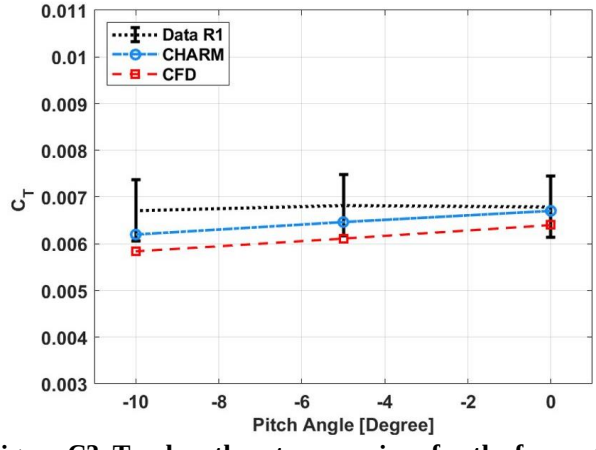

Figure C3. Tandem thrust comparison for the fore rotor at 3000 RPM and tunnel speed of ~20 ft/s (μ = 0.062).

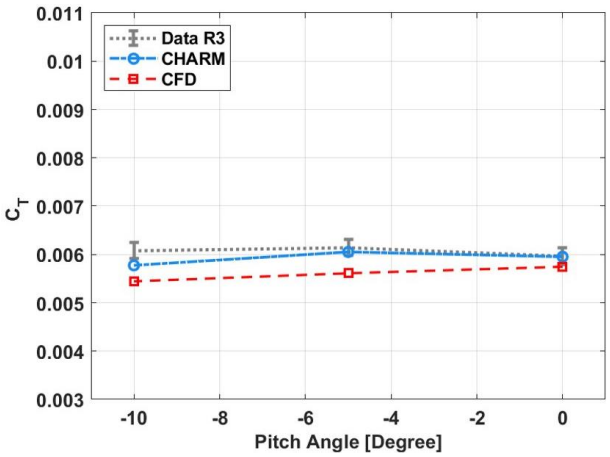

Figure C4. Tandem thrust comparison for the aft rotor at 3000 RPM and tunnel speed of ~20 ft/s (μ = 0.062).

ACKNOWLEDGMENTS

The authors thank Wayne Johnson, Ethan Romander, Sesi Kottapalli, and Dan Wachspress for their guidance and for reviewing this work. The authors would like to acknowledge Larry Meyn for completing load cell calibration, data post-processing, and uncertainty quantification, and Isabelle Pichay and Alex Sheikman for their assistance with the load cell calibration. In addition, the authors would like to thank William Warmbrodt and the RVLT Project for supporting this study. Resources supporting this work were provided by the NASA High-End Computing (HEC) Program through the NASA Advanced Supercomputing (NAS) Division at Ames Research Center.

REFERENCES

1. Russell, C., Theodore, C., Jung, J., and Glanser, B., "Wind Tunnel and Hover Performance Test Results for Multicopter UAS Vehicles," NASA/TM–2018–219758, Moffett Field, CA, February 2018.

2. Russell, C., and Conley, S., "The Multirotor Test Bed – A New NASA Test Capability for Advanced VTOL Rotorcraft Configurations," Vertical Flight Society 76th Annual Forum & Technology Display, Virtual, October 2020.

3. Silva, C., Johnson, W. R., Solis, E., Patterson, M. D., and Antcliff, K. R., "VTOL Urban Air Mobility Concept Vehicles for Technology Development," Aviation Technology, Integration, and Operations Conference, Atlanta, Georgia, June 2018.

4. Kopyt, N., Niemiec, R., and Gandhi, F., "Quadcopter Rotor Phasing for Minimization of Aircraft Vibratory Loads," VFS Aeromechanics for Advanced Vertical Flight Technical Meeting, San Jose, CA, January 2020.

5. Conley, S., Russell, C., Kallstrom, K., Shirazi, D., Pereyra, C., and Wright, S., "Multirotor Test Bed Second Wind Tunnel Entry Data Report," NASA/TM-2025-In progress, Moffett Field, CA, April 2025.

6. AIAA, "Recommended Practice: Calibration and Use of Internal Strain-Gage Balances with Application to Wind Tunnel Testing," Technical Report AIAA R-091A-2020, 2020.

7. Sukra Helitek, "AFTGen Final Report," SBIR Phase III Final Report 80NSSC18C0206, Sukra Helitek, 2020.

8. Nichols, R., and Buning, P. G., "User's Manual for OVERFLOW 2.3," NASA Langley Research Center, August 2010.

9. Johnson, W., "Technology Drivers in the Development of CAMRAD II," American Helicopter Society Aeromechanics Specialist Meeting, San Francisco, CA, January 1994.

10. Wachspress, D. A., Quackenbush, T. R., and Boschitsch, A. H., "Wind Tunnel Testing and Analysis of a Rigid, Variable Speed Rotor for eVTOL Applications," Journal of the American Helicopter Society, Vol. 48, (4), October 2003, pp. 223–235(13).

11. Quackenbush, T. R., Boschitsch, A. H., Wachspress, D. A., McKillip, R., and MacNichol, A., "Fast Analysis Methods for Surface-bounded Flows with Applications to RotorWake Modeling," American Helicopter Society 52nd Annual Forum, Washington DC, June 1996.

12. Bliss, D., and Quackenbush, T. R., "A New Methodology for Free Wake Analysis Using Curved Vortex Elements," Paper AIAA 10.2514/6.2020-0302, AIAA SciTech 2020 Forum, Orlando, FL, January 2020.

13. Quackenbush, T. R., Bliss, D., Wachspress, D., Boschitsch, A., and Chua, K., "A New Methodology for Free Wake Analysis Using Curved Vortex Elements," NASA Contractor Report 177611, Hampton, VA, October 1990.

14. Boschitsch, A., Curbishley, T., Quackenbush, T. R., and Teske, M., "Fast Panel Method for Potential Flows About Complex Geometries," Paper AIAA-96-0024, AIAA 34th Aerospace Sciences Meeting & Exhibit, Reno, NV, January 1996.

15. Boschitsch, A., Usab, W., and Epstein, R., "Fast Lifting Panel Method," Paper AIAA-99-3376, AIAA 14th Computational Fluid Dynamics Conference, Norfolk, VA, June 1999.

16. Quackenbush, T. R., Lam, C.-M. G., and Wachspress, D. A., "Computational Analysis of High Resolution

Unsteady Airloads for Rotor Aeroacoustics," NASA Contractor Report 194894, Hampton, VA, May 1994.

17. Diaz, P. V., and Yoon, S., "Computational Study of NASA's Quadrotor Urban Air Taxi Concept," AIAA SciTech Forum, Orlando, FL, January 2020.

18. Peters, N., and Shirazi, D., "On the Application of an Actuator Line Model for Rotorcraft Outwash Predictions," AIAA SciTech Forum, Orlando, FL, January 2025.

19. Ahmad, J. U., "Application of Rotor Disk Model in the OVERFLOW CFD Code," NASA/TM—20220005496, Moffett Field, CA, April 2022.

20. Wachspress, D., Whitehouse, G., Yu, K., Gilmore, P., Dorsett, M., and McClure, K., "A High Fidelity Brownout Model For Real-time Flight Simulations and Trainers," Proceedings of the 65th Annual American Helicopter Society Forum., 2009.

21. Conley, S., Russell, C., Shirazi, D., Kallstrom, K., Pereyra, C., and Wright, S., "An Experimental Investigation of Quadrotor Variations using NASA's Multirotor Test Bed," Vertical Flight Society 81st Annual Forum and Technology Display, Virginia Beach, VA, May 2025.

22. Schatzman, D., "Tunnel Survey and Calibration Report - 7- x 10-ft Wind Tunnel," U.S. Army Technical Report, A215-00-R0006, Moffett Field, CA, 2019.

23. Kallstrom, K., and Shirazi, D., "Airfoil Table Generation and Validation for the VR-12 and SSC-A09 Airfoils and Quadrotor Performance Prediction," Vertical Flight Society Sixth Decennial Aeromechanics Specialists' Conference, Santa Clara, CA, February 2024.